(2)

NORTHWESTERN UNIVERSITY

McCORMICK SCHOOL OF ENGINEERING AND APPLIED SCIENCE

DEPARTMENT OF MATERIALS SCIENCE

TECHNICAL REPORT #32

OFFICE OF NAVAL RESEARCH

JULY 1991

CONTRACT NO. N0014-80-C-116

CHANGES IN THE MACROSTRESSES AND MICROSTRESSES IN STEEL WITH FATIGUE

BY

R.A. Winholtz and J.B. Cohen

EVANSTON, ILLINOIS

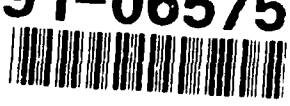

Changes in the Macrostresses and Microstresses in Steel with Fatigue

R.A. WINHOLTZ and J.B. COHEN

Department of Materials Science and Engineering, The Robert R. McCormick School of Engineering and Applied Science, Northwestern University, Evanston, IL 60208

Abstract

The residual stresses in both the ferrite and cementite phases of fatigued 1080 steel specimens with pearlite, spheroidite, and tempered martensite microstructures were measured with x-ray diffraction giving both the macrostresses and the microstresses. Specimens with no initial stresses showed little changes with fatigue. Specimens with initial macrostresses and with initial microstresses showed fading of the stresses, the fading being the slowest for the strongest microstructure. Hydrostatic microstresses are present after heat treatment due to the differential thermal properties of the cementite and ferrite.

1 Introduction

Residual stresses play an important role in the fatigue of engineering materials. Because fatigue cracks generally start at the surface, the residual stresses there are usually the most relevant. Compressive stresses in high stress areas are usually considered beneficial because they impede crack formation and growth. Tensile residual stresses on the other hand are detrimental because they aid crack formation and growth and can lead to stress corrosion cracking.

Previous work has shown that residual stresses can change or develop with fatigue loading [1-8]. References 5 and 6 give good reviews of the subject. In recent years it has become clear that in two phase materials both macrostresses and microstresses can exist [9,10]. With diffraction measurements it is possible to separate the macrostresses and microstresses and thus determine their individual changes with fatigue loading [7-11]. Noyan and Cohen measured the stresses in both the α and β phases of a two phase brass [7,11] and determined that with fatigue loading residual stresses were inhomogeneously distributed in the softer α phase of the material. Most work in this area, however, has assumed that the measured stresses were macrostresses and have ignored the possibility of microstresses in the fatigue of two phase materials. The differentiation between the macrostresses and microstresses is important because they could have different origins. Macrostresses, which must balance between macroscopic regions, are indicative of differences in behavior of the surface and interior of the specimen. In contrast, microstresses could develop throughout the specimen and would indicate differential behavior of the phases present.

Steel is still a very important engineering material and usually consists of two phases: ferrite and carbides, and thus, in general, both macrostresses and microstresses will be present. Microstresses have not often been measured in materials and their effect on fatigue life is not yet clear. In the low cycle fatigue of steel where the phases may be plastically deformed cyclically the microstresses change continuously, alternating signs with each half cycle, and the stress range in the stronger cementite phase is significantly higher [8]. In this work we observe the effect of high cycle fatigue loading on changes in both macrostresses and microstresses in order to characterize their individual roles in the fatigue of steel.

2 Theory

Stresses are measured with x-ray diffraction by measuring the changes in lattice spacing in different directions in the specimen using well established procedures [9]. These techniques permit the measurement of the total stress tensor in each phase of a material, the sum of the macrostress and the microstress tensors. By making measurements of the total stress tensor in each phase the macrostress and microstress tensors may be extracted [9,10].

Macrostresses are by definition the same in all the phases present in a material [9]. They arise from differential deformation of one region of a material with respect to another. These stresses vary slowly on a scale that is large compared to the material's microstructure. The macrostresses must balance to zero over any imaginary surface cutting the material in two. Microstresses, on the other hand, vary on the scale of the material's microstructure and must balance between the phases [9]. Microstresses arise from a variety of sources where the constituent phases behave

differently such as different plastic behavior or differences in the thermal expansion coefficients. For a two phase material we may write [9]

$$(1\text{-}f)\,{}^{\mu}\sigma^{\alpha}_{ij} + f\,{}^{\mu}\sigma^{\beta}_{ij} = 0\,. \tag{1}$$

Here ${}^{\mu}\sigma^{\alpha}_{ij}$ is the microstress in the first phase, ${}^{\mu}\sigma^{\beta}_{ij}$ is the microstress in the second phase, and f is the volume fraction of the second phase. The total stress in a phase that is measured with diffraction is the sum of the macrostress and the microstress:

$${}^{t}\sigma^{\alpha}_{ij} = {}^{M}\sigma_{ij} + {}^{\mu}\sigma^{\alpha}_{ij} \tag{2}$$

$${}^{t}\sigma^{\beta}_{ij} = {}^{M}\sigma_{ij} + {}^{\mu}\sigma^{\beta}_{ij}\,. \tag{3}$$

Here ${}^{M}\sigma_{ij}$ is the macrostress and ${}^{t}\sigma^{\alpha}_{ij}$ and ${}^{t}\sigma^{\beta}_{ij}$ are the total stresses which may be measured with diffraction. From these equations the macrostress and microstress tensors may be determined from stress measurements in each phase [9].

The total stress tensor in a phase may be determined with x-ray diffraction by precisely measuring changes in the lattice spacings in different directions in the specimen [10]. The lattice spacings give the strains in the specimen and the stresses can then be determined using the appropriate diffraction elastic constants [10,12]. The strain in a phase along any given direction, $e^{\alpha}_{\phi\psi}$ is given by

$$e^{\alpha}_{\phi\psi} = (d^{\alpha}_{\phi\psi} - d^{\alpha}_{0})/d^{\alpha}_{0}\,, \tag{4}$$

where $d^{\alpha}_{\phi\psi}$ is the lattice spacing in a given direction measured by diffraction and d^{α}_{0} is the unstressed lattice spacing. Using tensor coordinate transformations the strain $e^{\alpha}_{\phi\psi}$ may be written as

$$e^{\alpha}_{\phi\psi} = (d^{\alpha}_{\phi\psi} - d^{\alpha}_{0})/d^{\alpha}_{0} = \varepsilon^{\alpha}_{11}\cos^2\phi\sin^2\psi + \varepsilon^{\alpha}_{22}\sin^2\phi\sin^2\psi + \varepsilon^{\alpha}_{33}\cos^2\psi + \varepsilon^{\alpha}_{12}\sin 2\phi\sin^2\psi + \varepsilon^{\alpha}_{13}\cos\phi\sin 2\psi + \varepsilon^{\alpha}_{23}\sin\phi\sin 2\psi \quad . \tag{5}$$

Here $\varepsilon^{\alpha}_{ij}$ is the strain tensor referenced to the sample coordinate system S_i as shown in Figure 1 and the angles ϕ and ψ define a given direction relative to this sample coordinate system. By measuring a collection of $e^{\alpha}_{\phi\psi}$ the strain tensor in the specimen $\varepsilon^{\alpha}_{ij}$ may be determined by least squares [13]. The stresses are then obtained using Hooke's law:

$${}^{t}\sigma^{\alpha}_{ij} = \frac{1}{S^{\alpha}_{2}/2}\left[\varepsilon^{\alpha}_{ij} - \delta_{ij}\frac{S^{\alpha}_{1}}{S^{\alpha}_{2}/2 + 3S^{\alpha}_{1}}(\varepsilon^{\alpha}_{11} + \varepsilon^{\alpha}_{22} + \varepsilon^{\alpha}_{33})\right]. \tag{6}$$

Here S^{α}_{1} and $S^{\alpha}_{2}/2$ are the diffraction elastic constants [12] and δ_{ij} is the Kronecker delta function.

In this procedure determining accurate values of the unstressed lattice parameters can be problematical [14]. It has been shown [12] that the deviatoric stresses may be determined without accurate values of the unstressed lattice parameters of the constituent phases, while errors in the unstressed lattice parameters lead to errors in the hydrostatic component of the stress tensors only. If we rewrite Equation 5 in terms of the hydrostatic strain ε^{α}_{H} and deviatoric strain $'\varepsilon^{\alpha}_{ij}$, (where $\varepsilon^{\sigma}_{ij} = '\varepsilon^{\alpha}_{ij} + \delta_{ij}\varepsilon^{\alpha}_{H}$ and $\varepsilon^{\alpha}_{H} = (\varepsilon^{\alpha}_{11}+\varepsilon^{\alpha}_{22}+\varepsilon^{\alpha}_{33})/3$) and solve for $d^{\alpha}_{\phi\psi}$, we obtain:

$$
\begin{aligned}
d^{\alpha}_{\phi\psi} = \quad & \varepsilon^{\alpha}_{H}\, d^{\alpha}_{0} + d^{\alpha}_{0} \\
& + {}^{\prime}\varepsilon^{\alpha}_{11}\, d^{\alpha}_{0} \cos^2\phi \sin^2\psi \\
& + {}^{\prime}\varepsilon^{\alpha}_{22}\, d^{\alpha}_{0} \sin^2\phi \sin^2\psi \\
& + {}^{\prime}\varepsilon^{\alpha}_{33}\, d^{\alpha}_{0} \cos^2\psi \\
& + {}^{\prime}\varepsilon^{\alpha}_{12}\, d^{\alpha}_{0} \sin 2\phi \sin^2\psi \\
& + {}^{\prime}\varepsilon^{\alpha}_{13}\, d^{\alpha}_{0} \cos\phi \sin 2\psi \\
& + {}^{\prime}\varepsilon^{\alpha}_{23}\, d^{\alpha}_{0} \sin\phi \sin 2\psi \ . \qquad (7)
\end{aligned}
$$

We see clearly here that $d^{\alpha}_{\phi\psi}$ has no angular dependency on the hydrostatic strain. Thus one may not determine ε^{α}_{H} from just a collection of $d^{\alpha}_{\phi\psi}$ because there are two terms with no angular dependency, $\varepsilon^{\alpha}_{H} d^{\alpha}_{0}$ and d^{α}_{0}. Only the sum of these two terms may be determined and ε^{α}_{H} can only be determined by accurately knowing d^{α}_{0}. Further, the accuracy with which ε^{α}_{H} can be determined is limited by the accuracy to which d^{α}_{0} is known.

The deviatoric and hydrostatic stresses can then be obtained from the strains using

$$
{}^{t}\tau^{\alpha}_{ij} = {}^{\prime}\varepsilon^{\alpha}_{ij}/(S^{\alpha}_{2}/2) \qquad (8)
$$

$$
{}^{t}\tau^{\alpha}_{H} = \varepsilon^{\alpha}_{H}\, 3(S^{\alpha}_{2}/2)/[3\, S^{\alpha}_{2}/2\, (S^{\alpha}_{2}/2 + 3S^{\alpha}_{1})] \ . \qquad (9)
$$

Since the hydrostatic component of the stress tensor does not affect the plastic deformation, the deviatoric stress tensor is often adequate to describe the residual stress state with respect to mechanical loading such as fatigue. Also, any error in the hydrostatic stress due to the unstressed lattice parameter will be constant

and relative changes in this stress will be without this error. Therefore accurate values of the unstressed lattice parameter are not always needed for fruitful analysis.

Equations 1, 2, and 3 hold independently for the deviatoric and hydrostatic stress tensors which can also be separated into macrostress and microstress components.

The statistical errors in the deviatoric stress tensor will arise from the statistical errors in determining the lattice spacings from the measured peak positions and can be propagated through the least squares procedure in a straightforward manner [13]. The errors in the hydrostatic stress tensor, however, will be dominated by the uncertainty in d^{α}_{0}. Note that it is incorrect to propagate the error in d^{α}_{0} through Equation 4 to an error in each measured strain value $\varepsilon^{\alpha}_{\phi\psi}$, as has been done previously [15], because these errors are not independent of each other but are instead completely correlated. To correctly handle errors due to d^{α}_{0} we must work with Equation 7. From a least squares solution of Equation 7 we may determine a constant D which is equal to $\varepsilon^{\alpha}_{H} d^{\alpha}_{0} + d^{\alpha}_{0}$. This constant D will have a value of approximately d^{α}_{0} and will have its own statistical uncertainty arising from the propagation of uncertainties in $d^{\alpha}_{\phi\psi}$ through the least squares procedure. The error in ε_{H} due to d^{α}_{0} is then

$$STD(\varepsilon^{\alpha}_{H}) = STD(d^{\alpha}_{0})\,(D/d^{\alpha}_{0}{}^{2})^{2}\ . \qquad (10)$$

Propagating this error through Equation 9 and approximating D by d^{α}_{0} we have the error in the hydrostatic stress due to an error in d^{α}_{0}

$$STD(\sigma^{\alpha}_{H}) = 3(S^{\alpha}_{2}/2)/[3\,S^{\alpha}_{2}/2\,(S^{\alpha}_{2}/2 + 3S^{\alpha}_{1})]\ STD(d^{\alpha}_{0})/d^{\alpha}_{0}. \qquad (11)$$

The hydrostatic stress will also have an uncertainty due to the statistical error in D but this will in general be much smaller than the errors due to d^{α}_{0} and Equation 11 will dominate the error in ${}^{t}\tau^{\alpha}_{H}$.

3 Experimental Procedures

Fatigue specimens for this study were made from 1080 steel obtained from Amtex Steel Inc. (Chicago, IL) in the form of hot rolled plate. This steel has a near eutectoid composition. Results should be applicable to steels strengthened with other types of carbides.

Stress controlled fatigue loading was carried out at two stress levels, 276 and 345 MPa (40 and 50 ksi). Specimens for 276 MPa are shown in Figure 2a and those for 345 MPa are shown in Figure 2b. The fatigue specimens were machined from the center of the plate with the rolling direction corresponding to the loading axis. After machining, the specimens were polished through 600 grit with SiC paper, the final scratches running along the loading direction of the specimens.

Specimens were heat treated to give three different microstructures: pearlite, spheroidite, and tempered martensite. The heat treatments are given in Table 1. The surface preparation and heat treatment of the samples was designed to give smooth surface finishes free of residual stresses introduced by mechanical polishing. The specimens were thus first machined and polished and then heat treated to remove any residual stresses due to the machining and polishing. The tempered martensite specimens were repolished between quenching and tempering to remove the scale that formed on quenching into oil.

The volume fraction of the cementite phase f is needed to separate the

macrostresses and microstresses. The volume fraction of the cementite was measured for each microstructure from the ratio of the integrated intensities of the 110, 200, and 211 ferrite diffraction peaks to the integrated intensities of the 121, 210, 002, 201, 211, 102, 112, 131, 221, 401, 133, and 250 cementite peaks [16,17]. The values of f are shown in Table 2. The errors for each value of f were determined from the standard deviations in the individual normalized peak intensities. The pearlite and spheroidite have the percentage of cementite that would be expected for a 1080 steel. These measurements show that some decarburization of the surface took place in the tempered martensite specimens during quenching from the furnace to the oil bath as there is only 5.7% cementite. Deeper into the specimen the volume fraction of cementite is 11.2% (±6.2) which is what would be expected for a 1080 steel. The value at the surface where the diffraction measurements were made was used for all the stress calculations.

Much of the previous work has been done with bending or rotating fatigue loading [1,2,5,6]. While this geometry is useful for applying a large number of cycles in a reasonable amount of time, the stress loading is uneven across the cross section. Since stress gradients are present residual macrostresses and microstresses may form which are due to the loading method and not due to processes inherent in the fatigue process. In the study, fatigue loading was done on an MTS 100 kN servo-hydraulic fatigue machine at room temperature. The specimen grips were aligned by melting a Woods metal bath holding the lower grip and letting it solidify while gripping a standard alignment plate. This will minimize any bending moments on the specimen during fatigue loading. The specimens were loaded in fully reversed (R=-1) stress

control with a sinusoidal waveform at 10 Hz. In all cases the fatigue was halted after a compressive half cycle.

Four specimens were tested at 276 MPa; one of each microstructure in the as heat treated condition and a fourth with a spheroidite microstructure that had been shot peened to introduce compressive stresses in the surface region. Shot peening is known to significantly improve the fatigue life of components. Shot peening was done by The Metal Improvement Company (Addison, IL). The specimen was shot peened on all four sides of the gauge section to an Almen A arc height of 0.1651 mm (0.0065 in) with #230 steel shot. The surface was left in the state produced by the shot peening for the x-ray measurements. The spheroidite microstructure was the only one in which the cementite peaks were still resolvable after shot peening.

Nine specimens were tested at 345 MPa, three for each microstructure. For each microstructure one specimen was fatigued in the as heat treated condition, one was fatigued after an initial plastic tensile deformation, and one was fatigued after an initial plastic compressive deformation. Because the ferrite deforms preferentially to the cementite the plastic tensile deformation gives the ferrite a compressive microstress and the cementite a tensile microstress while the plastic compressive deformation gives the opposite [8,16]. The microstresses were induced to examine the effect of fatigue loading. The deformations were done on the same fatigue machine that was used for applying the fatigue loads. The pearlite and spheroidite microstructures were deformed to a strain of $\pm$ 0.0075 and the tempered martensite to a strain of $\pm$ 0.005.

Stress measurements were performed using methods described in detail previously [8,16]. Measurements were made with Cr radiation using the 211

diffraction peak at approximately 156° 2θ for the ferrite phase and the 250 peak at approximately 148° 2θ for the cementite phase. The diffraction peaks were measured at 31 different ϕ and ψ tilts and fit with pseudo-Voigt functions [18] to determine the peak positions. The stresses were then determined by a least-squares procedure [13,16]. The total time for one stress measurement was about 20 hours. Specimens were removed from the fatigue machine and the stresses measured. The stress tensors are oriented such that τ_{11} corresponds to the loading direction on the fatigue specimen and τ_{33} is normal to the specimen surface. The x-ray elastic constants used were measured for both phases in each microstructure and reported previously [8].

In order to estmate the hydrostatic components of the stress tensors the lattice spacing of the exact phases present in the specimens must be measured in a stress free condition. To do this for these specimens the cementite was chemically extracted from the steel for each microstructure. Pieces of the grip ends of the specimens were soaked in a solution of four parts methyl alchohol and one part nitric acid for approximately an hour. The solution preferentially disolved the ferrite matrix leaving cementite particles on the surface. The pieces were then removed and rinsed in water being carefull to avoid washing the cementite off. Some of the cementite was then lifted off with a piece of cellophane tape. This process was repeated 3 or 4 times with the same piece of tape in order to get enough cementite particles to measure the unstressed lattice spacing. Some silicon powder was next also sprinkled onto the tape along with the cementite particles in order to give a cubic crystal structure in the diffraction pattern so that the specimen displacement measured and minimized by adjusting the specimen displacement until all of the silicon peaks gave the same lattice parameter [10]. The tape was mounted on the diffractometer,

aligned, and the unstressed lattice spacing measured for each microstucture measured with the same experimental parameters as for the stress measurements. The peak postion was determined by fitting pseudo-Voigt function to the diffraction data. The diffraction patterns were checked to make sure that the ferrite peaks were absent.

Since attempts to similarly chemically isolate the ferrite phase failed, the values for the unstressed lattice parameters were computed using equations of stress equilibrium. With x-ray diffraction the macrostress ${}^{M}\sigma_{33}$ must be zero within the diffraction volume because it must be zero at the surface and have no gradients into the specimen in the S_3 direction [9,10]. The macrostresses and microstresses were determined using the measured unstressed lattice parameter for the cementite and an initial guess for the ferrite parameter. The value for the ferrite was adjusted until the macrostress ${}^{M}\sigma_{33}$ was zero. This value was then used for the unstressed lattice parameter. This numerical procedure was performed on the data for specimens F3, F5, and F7 at 0 fatigue cycles and the resulting unstressed ferrite lattice parameter used for all of the other tests.

The errors in d^{c}_{0} come directly from the statistical errors in the fit of the diffraction peak of the unstressed powder. We must also estimate an error in d^{α}_{0} from the procedure used to obtain it. Since ${}^{M}\sigma_{33}$ must be zero we see from Equation 1 that the microstresses ${}^{\mu}\sigma^{\alpha}_{ij}$ and ${}^{\mu}\sigma^{c}_{ij}$ must be of opposite sign and must sum to zero when weighted by their volume fraction. Any error in d^{c}_{0} will cause an error in ${}^{\mu}\sigma^{c}_{ij}$ which will force an error in ${}^{\mu}\sigma^{\alpha}_{ij}$ to satisfy Equation 1 which causes an error in d^{α}_{0}. The error in ${}^{\mu}\sigma^{\alpha}_{ij}$ due to the error in d^{c}_{0} will be smaller than the error in ${}^{\mu}\sigma^{c}_{ij}$ by the ratio of their volume fractions (see Equation 1). Since the elastic constants of the ferrite and cementite are nearly the same [8] the ratio of the error in d^{α}_{0} to the error in d^{c}_{0}

will be equal to the ratio of their volume fractions. Since there is a smaller volume fraction of the cementite phase errors in d^{α}_0 due to this procedure will be smaller than the errors in d^{c}_0. To account for uncertainties in the elastic constants and as a conservative estimate the error in d^{c}_0 was also assigned to d^{α}_0.

Errors in the stresses are reported as the sum in quadrature of the statistical, instrumental, and volume fraction errors for the deviatoric stress tensors and of the d_0 and volume fraction errors for the hydrostatic stresses. The statistical errors arise from the counting statistics of determining the diffraction peak locations and the instrumental errors arise primarily from the x-ray beam divergence and sample displacement [10].

4 Results and Discussion

In Table 2 the unstressed lattice parameters for the different microstructures are presented as well as the measured volume fractions of the cementite phase. Within the errors determined from the fit to the diffraction peak the unstressed lattice parameters are the same for each microstructure but are little bit smaller than the value of 1.1917 Å given in the literature [19]. Table 3 gives the deviatoric macrostress and microstress tensors as well as the hydrostatic stresses measured in the specimens fatigued at 276 MPa. Figure 3 shows the deviatoric stresses τ_{11} along the loading direction for the three different microstructures each in the as heat treated condition. We see that the initial stresses are small and that the changes with fatigue are also small, the absolute value of all stresses remaining under 40 MPa.

Figure 4 shows the changes in the residual stresses in a spheroidized and shot peened specimen. This specimen proved to be the most difficult to measure the

stresses in the cementite phase because the shot peening broadened the diffraction peaks almost completely obscuring the 250 cementite peak under the 211 ferrite peak. Before fatigue loading the specimen has relatively large compressive macrostresses and only small microstresses. The compressive macrostresses in the surface layer must then provide the improved fatigue resistance in the shot peened material. The microstresses are much smaller than the compressive macrostresses so that both phases have significant compressive stresses in the shot peened material. As the specimen was fatigued the macrostress relaxed indicating that the interior of the specimen is elongating and the surface is contracting relative to each other. From Table 3 we see that the compressive stresses in the sample surface perpendicular to the loading direction ${}^{M}\tau_{22}$ also fade with fatigue.

Table 3d lists the hydrostatic components of the macrostress and microstress tensors. The hydrostatic macrostress ${}^{M}\tau_{H}$ should be opposite in sign to ${}^{M}\tau_{33}$ in each case because they must sum to make ${}^{M}\sigma_{33}$ equal zero to satisfy equilibrium relations. For specimens F5, F3, and F7 with no fatigue cycles this condition is exactly met because it was used to determine the unstressed lattice spacing in the ferrite. In the other specimens this condition is met within the error bars.

In the as heat treated specimens the microstresses will be thermal in nature, arising from the precipitation, growth, thermal expansion, and thermal relaxation of the ferrite and cementite phases for the thermal history of the specimens. Laszlo and Nolle [20] and Kagawa et. al [21] have examined the thermal coeffiecients of expansion of ferrite and cementite by making dilatometric measurements on pearlitic steels with different amounts of carbon and hence different amounts of cementite.

Both found that the thermal coefficient of expansion was smaller in cementite than in ferrite. Thus in cooling from a high temperature one would expect to the cementite to have a hydrostatic tensile stress and the ferrite to have a hydrostatic compressive stress. This is indeed seen in the as heat treated pearlite and spheroidite. In contrast the tempered martensite has a compressive hydrostatic microstress in the cementite in the as heat treated condition. In tempered martensite where the cementite particles precipitate and grow in an already formed matrix thermal expansion coefficient calculations seem to be inappropriate.

Following Laszlo and Nolle [20] in taking a thermal coefficient of expansion differenc of $\Delta\alpha = \alpha^{\alpha}-\alpha^{c} = 2.25\text{x}10^{-6}/\text{K}$ and a temperature drop of about 680 K (973 K to room temperature) an average thermal hydrostatic tensile stress of 663 MPa is computed. This value is high but within reasonable agreement with the measured value for the cementite in the pearlite of 502 MPa but is much too high for the cementite in spheroidite which is measured to be about 188 MPa. This calculation, however, does not take into account any thermally activated stress relaxation taking place as the material cools from the reference temperature. Such processes will certianly take place and accounts for the lowered stresses observed in the pearlite and spheroidite; as the pearlitic specimens were cooled in argon from the autenitizing temperature while the spheroiditic specimens were allowed to cool in vacuum from 923 K we may infer that the pearlitic specimens cooled faster and therefore had less time at elevated temperatures for stress relaxation to occur. This accounts for the higher hydrostatic microstresses in the pearlite. However, more quantitative comparisons are not possible because the exact cooling rates were not measured. The amount of relaxation will depend upon the complete cooling rate

history and cannot be computed without knowing specimen cooling rates and measuring rate constants for the relaxation processes.

Finally, we note that no significant changes are seen in the hydrostatic microstresses with fatigue loading at 276 MPa.

Table 4 lists the stress tensors measured in the specimens fatigued at 345 MPa. The specimens with the initial tensile deformation show large tensile microstresses in the cementite phase while those with an initial compressive deformation show large compressive microstresses in the cementite. Equation 1 shows that the microstresses must be much larger in the cementite because it has a much smaller volume fraction. Figures 5, 6, and 7 show the residual stresses along the loading direction versus the number of fatigue cycles. As was the case for fatigue at 276 MPa the specimens with no initial stresses show little change with fatigue. The microstresses initially present in the specimens fade with fatigue loading just as the macrostresses in the shot peened specimen did. The rate of fading is inversely related to the strength associated with the microstructure; the stresses in the pearlite and spheroidite relax very rapidly while the stresses in the tempered martensite relax at a slower rate. Even in the tempered martensite though, there is significant relaxation of the residual stresses after only 100 cycles. We also note the the rate of relaxation is independent of which phase has the tensile microstresses and which phase has the compressive microstresses.

With the hydrostatic microstresses shown in Table 4d the only difference we see from the specimens fatigued at 276 MPa is that the thermal microstresses in the pearlite are removed by the plasitc deformation and higher load range in fatigue at 345 MPa. The size of the errors in relation to the measured hydrostatic microstresses

in the measurements prevents any conclusions from being drawn in the other microstructures.

In previous studies [1-5] residual stresses develop with fatigue loading but it is unclear whether they are macrostresses or microstresses because the stresses were measured in only one phase of the material. In this study we have observed the fading of preexisting residual stresses but saw no evidence of residual stresses forming with fully reversed uniaxial fatigue loading. As previously reported [7,8], microstresses can develop with fatigue when the phases deform significantly relative to each other during the fatigue loading. In the low cycle fatigue of steel the microstresses change continuously as the ferrite deforms preferentially to the cementite during the cyclic deformation [8]. Noyan and Cohen [7] also reported changes in microstresses during the fatigue of a two phase brass where the residual stresses developed to inhomogeneously in the softer α phase. Different fatigue or specimen conditions may also account for the development of residual stresses during fatigue. Nonuniform stress loading such as in bending fatigue may cause a nonuniform material response and cause macrostresses to develop during fatigue. A nonzero mean stress during fatigue was observed to cause residual stresses in Reference 3. A nonuniform microstructure, such as in a rolled plate, may also lead to the development of residual macrostresses because of a differences in the material response to fatigue loading over the cross section. In this study though, in the tempered martensite specimens where a composition gradient exists in the surface region due to some decarburization no residual macrostresses develop as might be expected due to different material behavior at the surface and in the interior.

5 Conclusions

1) In as heat treated specimens of pearlite, spheroidite, and tempered martensite with no initial residual stresses no development of residual stresses was seen for fully reversed uniaxial fatigue loading.

2) Macrostresses initially present fade with fatigue (as for example, after shot peening).

3) Both initial compressive and tensile microstresses initially present fade with fatigue. The rate of fading does not depend upon which phase is in tension and which is in compression.

4) Fading of the microstresses is the slowest for the strongest microstructure. Even in tempered martensite, however, significant fading of the stresses takes place after only 100 fatigue cycles.

5) Hydrostatic microstresses are present in pearlite and spheroidite in the as heat treated condition which arise from the coefficient of thermal expansion mismatch between the ferrite and cementite. These stresses are smaller than predicted indicating that stress relaxation takes place during cooling from elevated temperatures.

Acknowledgments

The support of the Office of Naval Research under Grant No. N00014-80-C0116 is gratefully acknowledged. We thank Mr. James Wandell of the Metal Improvement Co. for the shot peening done in this study. The x-ray and fatigue work made use of the Northwestern X-ray Diffraction and Fatigue facilities which are supported in part by the National Science Foundation through the Northwestern University Material Research Center, Grant No. DMR 8821571. This research represents a portion of a thesis submitted (by R.A.W.) to Northwestern University in partial fulfillment of the requirements for the Ph.D. degree.

References

1. S. Taira and Y. Murakami, *4th Japan Congress on Testing Materials* (1961) 5.

2. S. Taira and K. Honda, *5th Japan Congress on Testing Materials* (1962) 8.

3. M. McClinton and J.B. Cohen, *Mat. Sci. Engr.*, 56 (1982) 259.

4. H.K. Kuo and J.B. Cohen, *Mat. Sci. Engr.*, 61 (1983) 127-136.

5. I.C. Noyan and J.B. Cohen, in E. Ku la, V. Weiss (eds.), *Residual Stress and Stress Relaxation*, Plenum Press, New York, 1982, p. 1.

6. M.R. James and W.L. Morris, in *Residual Stress for Designers and Metallurgists*, ASM, 1981, 169.

7. I.C. Noyan and J.B. Cohen, *Mat. Sci. Engr.*, 79, (1986) 149.

8. R.A. Winholtz and J.B. Cohen, Submitted to *Met. Trans.*

9. I.C. Noyan, *Met. Trans. A*, 14A (1983) 1907.

10. I.C. Noyan and J.B. Cohen, *Residual Stress: Measurement by Diffraction and Interpretation*, Springer-Verlag, New York, 1987.

11. I.C. Noyan and J.B. Cohen, *Mat. Sci. Engr.*, 75 (1985) 179.

12. K. Perry, I.C. Noyan, P.J. Rudnik, and J.B. Cohen, *Adv. X-ray Anal.*, 27 (1984) 159.

13. R.A. Winholtz and J.B. Cohen, *Aust. J. Phys.*, 41 (1988) 189.

14. I.C. Noyan, *Adv. X-ray Anal.*, 28, (1985) 178.

15. P.Rudnik and J.B. Cohen, *Adv. X-ray Anal.*, 29 (1986) 79.

16. R.A. Winholtz and J.B. Cohen, *Adv. X-ray Anal.*, 32, 341.

17. A.F. Giamei and E.J. Freise, *Trans. AIME*, 1967, 239, 1676.

18. G.K. Wertheim, M.A. Butler, K.W. West, and D.N.E. Buchanan, *Rev. Sci. Instrum.*, 45 (1974) 1369.

19. E.J. Fasiska and G.A. Jeffrey, *Acta Cryst.*, 19 (1965) 463.

20. F. Laszlo and H. Nolle, *J. Mech. Phys. Solids*, 7 (1959) 193.

21. A. Kagawa, T. Okamoto, and H. Matsumoto, *Acta Met.*, 35 (1987) 797.

Table 1. Specimen Heat Treatments.

Microstructure	Heat Treatment
Pearlite	Austenitize at 1073 K for 15 min. in argon. Allowed to cool in argon outside the hot zone of the furnace.
Spheroidite	Heat at 973 K for 10 hours in vacuum of 10^{-6} Torr.
Tempered Martensite	Austenitize at 1073 K for 15 min in argon. Quench in oil. Temper at 773 K for one hour.

Table 2. Unstressed lattice parameters d_0 and the volume fraction of cementite f. d^c_0 is for the 250 cementite peak and d^α_0 is for the 211 ferrite peak.

Microstucture	d^c_0 (Å)	d^α_0 (Å)	f(%)
Spheroidite	1.190964 (0.000075)	1.170030 (0.000075)	14.6 (4.7)
Pearlite	1.191190 (0.000140)	1.170251 (0.000140)	12.9 (5.4)
Tempered Martensite	1.191126 (0.000103)	1.170141 (0.000103)	5.7 (4.0)

Numbers in parentheses are the errors in the lattice spacings and volume fractions.

Table 3. Stresses after fatigue at 276 MPa.

(a) Deviatoric Macrostresses (MPa)

Specimen		Cycles	$^{M}\tau_{11}$	$^{M}\tau_{22}$	$^{M}\tau_{33}$	$^{M}\tau_{12}$	$^{M}\tau_{13}$	$^{M}\tau_{23}$
F5	Pearlite	0	16 (13)	22 (13)	-38 (11)	-1 (1)	-1 (0.2)	-1 (0.2)
		1000	-13 (13)	31 (14)	-18 (11)	2 (1)	-1 (0.2)	0 (0.2)
		10000	-14 (13)	15 (13)	-1 (11)	0 (1)	0 (0.2)	0 (0.2)
		20000	-4 (13)	10 (13)	-7 (11)	-2 (1)	0 (0.2)	0 (0.2)
		40000	-3 (13)	17 (13)	-14 (11)	1 (1)	1 (0.3)	0 (0.2)
		80000	8 (13)	15 (13)	-22 (11)	1 (1)	0 (0.2)	1 (0.3)
		160000	9 (13)	9 (13)	-18 (11)	-3 (1)	0 (0.3)	1 (0.3)
		400000	12 (13)	7 (13)	-19 (11)	0 (1)	-1 (0.3)	0 (0.3)
F3	Spheroidite	0	0 (13)	5 (13)	-6 (11)	5 (1)	0 (0.2)	0 (0.1)
		100	3 (13)	1 (13)	-4 (11)	0 (1)	0 (0.2)	0 (0.2)
		1000	19 (13)	-15 (13)	-4 (11)	2 (1)	-2 (0.3)	-1 (0.2)
		10000	20 (13)	-16 (13)	-4 (11)	2 (1)	0 (0.2)	0 (0.2)
		79670*	2 (13)	-6 (13)	4 (11)	6 (1)	0 (0.2)	0 (0.2)
F7	Tempered Martensite	0	4 (14)	5 (14)	-9 (12)	1 (1)	-1 (0.6)	1 (0.5)
		1000	0 (14)	4 (14)	-4 (12)	0 (1)	0 (0.3)	0 (0.3)
		10000	2 (14)	3 (14)	-5 (12)	0 (1)	0 (0.3)	0 (0.3)
		100000	-1 (14)	4 (14)	-3 (12)	1 (1)	-1 (0.3)	-1 (0.3)
F2	Spheroidite Shot Peened	0	-138 (17)	-190 (21)	327 (23)	9 (5)	4 (2.3)	0 (1.6)
		1000	-118 (17)	-147 (17)	264 (20)	14 (4)	0 (2.7)	2 (1.7)
		11000	-78 (21)	-138 (25)	216 (25)	5 (6)	1 (2.7)	2 (1.9)
		100000	-58 (20)	-72 (23)	130 (21)	-8 (6)	7 (1.7)	3 (1.9)

Table 3. Stresses after fatigue at 276 MPa.

(b) Deviatoric Microstresses Ferrite (MPa)

Specimen		Cycles	$^{M}\tau^{\sigma}_{11}$	$^{M}\tau^{\sigma}_{22}$	$^{M}\tau^{\sigma}_{33}$	$^{M}\tau^{\sigma}_{12}$	$^{M}\tau^{\sigma}_{13}$	$^{M}\tau^{\sigma}_{23}$
F5	Pearlite	0	1 (13)	1 (13)	-2 (11)	0 (0.3)	0 (0.1)	0 (0.1)
		1000	2 (13)	-3 (13)	0 (11)	0 (0.4)	0 (0.2)	0 (0.1)
		10000	1 (13)	-1 (13)	0 (11)	1 (0.5)	0 (0.2)	0 (0.2)
		20000	0 (13)	0 (13)	0 (11)	0 (0.4)	0 (0.2)	0 (0.2)
		40000	-1 (13)	-1 (13)	2 (11)	0 (0.4)	-1 (0.3)	0 (0.2)
		80000	-2 (13)	-1 (13)	3 (11)	0 (0.6)	0 (0.2)	-1 (0.3)
		160000	-3 (13)	0 (13)	3 (11)	2 (0.6)	0 (0.2)	0 (0.2)
		400000	-3 (13)	0 (13)	3 (11)	0 (0.6)	0 (0.2)	0 (0.2)
F3	Spheroidite	0	0 (13)	0 (13)	0 (11)	1 (0.4)	0 (0.1)	0 (0.1)
		100	1 (13)	-1 (13)	0 (11)	0 (0.4)	0 (0.2)	0 (0.1)
		1000	2 (13)	-2 (13)	0 (11)	1 (0.5)	0 (0.2)	-1 (0.2)
		10000	5 (13)	-3 (13)	-2 (11)	2 (0.7)	0 (0.2)	0 (0.2)
		79670*	1 (13)	0 (13)	-1 (11)	1 (0.5)	-1 (0.2)	0 (0.2)
F7	Tempered Martensite	0	-1 (13)	0 (13)	1 (12)	0 (0.8)	1 (0.5)	-1 (0.4)
		1000	1 (14)	-2 (14)	0 (12)	0 (0.4)	0 (0.2)	0 (0.2)
		10000	0 (14)	-1 (14)	1 (12)	0 (0.5)	0 (0.2)	0 (0.2)
		100000	1 (14)	-1 (14)	0 (13)	0 (0.8)	0 (0.3)	0 (0.2)
F2	Spheroidite Shot Peened	0	2 (18)	18 (21)	-20 (14)	-6 (7.7)	6 (2.6)	5 (1.6)
		1000	14 (18)	4 (20)	-19 (14)	-8 (7.7)	8 (3.0)	-2 (1.6)
		11000	-1 (23)	23 (24)	-22 (17)	1 (5.4)	7 (2.9)	1 (1.9)
		100000	7 (21)	13 (24)	-20 (17)	9 (5.8)	2 (1.7)	1 (1.9)

Table 3. Stresses after fatigue at 276 MPa.

(c) Deviatoric Microstresses Cementite (MPa)

Specimen		Cycles	$^{\mu}\tau^{c}_{11}$	$^{\mu}\tau^{c}_{22}$	$^{\mu}\tau^{c}_{33}$	$^{\mu}\tau^{c}_{12}$	$^{\mu}\tau^{c}_{13}$	$^{\mu}\tau^{c}_{23}$
F5	Pearlite	0	-7 (16)	-7 (16)	14 (13)	0 (2)	1 (1)	1 (1)
		1000	-15 (17)	18 (17)	-3 (14)	3 (2)	2 (1)	0 (1)
		10000	-6 (19)	5 (19)	0 (16)	-3 (3)	1 (1)	2 (1)
		20000	-1 (19)	-2 (19)	2 (16)	-2 (3)	3 (1)	2 (1)
		40000	7 (19)	5 (18)	-12 (16)	3 (3)	5 (1)	2 (1)
		80000	14 (24)	4 (24)	-17 (19)	-1 (4)	0 (1)	4 (1)
		160000	19 (25)	-2 (24)	-17 (19)	-12 (4)	2 (2)	4 (2)
		400000	17 (31)	2 (25)	-19 (19)	3 (4)	-1 (1)	-2 (2)
F3	Spheroidite	0	0 (15)	2 (15)	-2 (12)	-3 (2)	-1 (1)	0 (1)
		100	-5 (15)	7 (15)	-2 (13)	3 (2)	-1 (1)	0 (1)
		1000	-12 (16)	11 (16)	1 (13)	-3 (3)	-2 (1)	3 (1)
		10000	-27 (16)	17 (16)	11 (13)	-11 (3)	0 (1)	-3 (1)
		79670*	-5 (16)	0 (16)	5 (13)	-6 (2)	3 (1)	3 (1)
F7	Tempered Martensite	0	17 (31)	5 (30)	-22 (34)	-2 (7)	-12 (3)	9 (3)
		1000	-22 (36)	27 (37)	-5 (42)	-3 (7)	-2 (3)	2 (3)
		10000	-5 (33)	17 (33)	-12 (37)	-5 (7)	-2 (3)	-2 (3)
		100000	-11 (32)	10 (34)	0 (38)	0 (7)	-1 (3)	-1 (3)
F2	Spheroidite Shot Peened	0	-14 (64)	-107 (74)	121 (49)	22 (23)	-34 (6)	-30 (7)
		1000	-80 (52)	-20 (58)	100 (39)	46 (17)	-49 (6)	8 (6)
		11000	3 (109)	-132 (112)	129 (78)	-7 (32)	-42 (11)	-8 (11)
		100000	-41 (99)	-76 (120)	117 (79)	-51 (34)	-12 (10)	-6 (11)

Table 3. Stresses after fatigue at 276 MPa.

(d) Hydrostatic Stresses (MPa)

Specimen		Cycles	μ_{T_R}	$\mu_{T^C_R}$	$\mu_{T^C_R}$
F5	Pearlite	0	38 (91)	-74 (39)	502 (165)
		1000	1 (92)	-82 (42)	554 (166)
		10000	-36 (89)	-56 (34)	378 (164)
		20000	-106 (88)	-44 (30)	298 (163)
		40000	-86 (88)	-55 (33)	373 (164)
		80000	-31 (90)	-65 (36)	440 (164)
		160000	57 (87)	-70 (24)	475 (162)
		400000	64 (87)	-77 (24)	517 (162)
F3	Spheroidite	0	6 (48)	-32 (16)	188 (70)
		100	27 (48)	-31 (16)	184 (70)
		1000	21 (48)	-31 (15)	179 (70)
		10000	-30 (47)	-11 (12)	67 (70)
		79670*	-42 (47)	-5 (12)	30 (70)
F7	Tempered Martensite	0	9 (48)	0 (6)	-4 (106)
		1000	47 (48)	9 (9)	-151 (106)
		10000	47 (48)	9 (9)	-151 (106)
		100000	62 (47)	10 (6)	-164 (106)
F2	Spheroidite Shot Peened	0	-537 (47)	14 (12)	-82 (70)
		1000	-382 (47)	-2 (12)	9 (69)
		11000	-302 (52)	12 (12)	-68 (70)
		100000	-160 (47)	-3 (12)	17 (70)

Numbers in parentheses are the sum in quadrature of the instrumental, statistical, and volume fraction errors.

*Indicates that the specimen broke.

Table 4. Stresses after fatigue at 345 MPa.

(a) Deviatoric Macrostresses (MPa)

Specimen		Cycles	$^{M}\tau_{11}$	$^{M}\tau_{22}$	$^{M}\tau_{33}$	$^{M}\tau_{12}$	$^{M}\tau_{13}$	$^{M}\tau_{23}$
A47	Pearlite	0	16 (13)	22 (13)	-38 (11)	-1 (1)	-1 (0.2)	-1 (0.2)
	No initial	190	18 (13)	-6 (13)	-11 (11)	-1 (1)	1 (0.2)	-3 (0.2)
	strain	27850*	-7 (13)	-13 (13)	20 (18)	-4 (1)	-2 (0.2)	6 (0.2)
A45	Pearlite	0	-13 (25)	16 (18)	-3 (18)	-18 (6)	-5 (2.1)	-4 (1.9)
	+0.0075	100	15 (13)	-6 (13)	-9 (11)	0 (1)	0 (0.2)	-1 (0.2)
	initial strain	30600*	13 (13)	-3 (13)	-10 (11)	-3 (1)	0 (0.2)	-1 (0.2)
A46	Pearlite	0	0 (21)	15 (16)	-15 (13)	-3 (1)	-3 (1.4)	-3 (0.8)
	-0.0075	100	20 (13)	-4 (13)	-16 (11)	-1 (1)	1 (0.3)	-1 (0.3)
	initial strain	24420*	4 (13)	-5 (13)	1 (11)	2 (1)	-2 (0.2)	0 (0.2)
A19	Spheroidite	0	-2 (13)	2 (13)	1 (11)	-1 (1)	0 (0.2)	0 (0.2)
	No initial	100	-10 (13)	13 (13)	-3 (11)	1 (1)	0 (0.2)	0 (0.2)
	strain	10390*	-14 (13)	-2 (13)	16 (11)	5 (1)	-1 (0.2)	-1 (0.2)
A20	Spheroidite	0	10 (18)	-15 (16)	5 (12)	2 (1)	-2 (0.5)	-1 (0.4)
	+0.0075	100	-8 (13)	9 (13)	-1 (11)	1 (1)	-1 (0.2)	0 (0.2)
	initial strain	12870*	11 (13)	4 (13)	-15 (11)	5 (1)	-1 (0.2)	-1 (0.2)
A26	Spheroidite	0	-21 (19)	21 (16)	0 (13)	-2 (1)	0 (0.4)	-2 (0.4)
	-0.0075	100	-10 (13)	10 (13)	0 (11)	-2 (1)	0 (0.2)	0 (0.2)
	initial strain	15500*	-1 (13)	-8 (13)	9 (11)	4 (1)	2 (0.2)	4 (0.2)
A42	Temp. Mart.	0	4 (14)	5 (14)	-9 (12)	1 (1)	-1 (0.6)	1 (0.5)
	No initial	100	22 (14)	-6 (14)	-16 (13)	-1 (1)	0 (0.3)	-1 (0.3)
	strain	99910	-9 (14)	10 (14)	-1 (13)	1 (1)	0 (0.3)	0 (0.4)
A37	Temp. Mart.	0	-104 (15)	17 (15)	87 (13)	-5 (2)	-2 (0.6)	2 (0.8)
	+0.005	100	-37 (14)	6 (14)	31 (12)	-2 (1)	1 (0.4)	-1 (0.4)
	initial strain	100000	-37 (14)	11 (14)	26 (12)	-1 (1)	-1 (0.4)	0 (0.4)
A41	Temp. Mart.	0	72 (15)	6 (14)	-78 (14)	8 (1)	-2 (0.4)	0 (0.4)
	-0.005	100	23 (14)	13 (14)	-36 (13)	7 (1)	-2 (0.4)	-2 (0.4)
	initial strain	100000	20 (14)	14 (14)	-34 (13)	6 (1)	-2 (0.4)	-1 (0.4)

Table 4. Stresses after fatigue at 345 MPa.

(b) Deviatoric Microstresses Ferrite (MPa)

Specimen		Cycles	$\mu\tau^{\alpha}_{11}$	$\mu\tau^{\alpha}_{22}$	$\mu\tau^{\alpha}_{33}$	$\mu\tau^{\alpha}_{12}$	$\mu\tau^{\alpha}_{13}$	$\mu\tau^{\alpha}_{23}$
A47	Pearlite	0	1 (13)	1 (13)	-2 (11)	0 (0.3)	0 (0.1)	0 (0.1)
	No initial	190	9 (13)	-6 (13)	-3 (11)	-1 (0.3)	1 (0.1)	1 (0.1)
	strain	27850*	11 (13)	-7 (13)	-4 (11)	1 (0.4)	0 (0.2)	1 (0.2)
A45	Pearlite	0	-54 (27)	22 (18)	32 (19)	13 (5.7)	5 (2.0)	4 (1.9)
	+0.0075	100	7 (13)	-5 (13)	-3 (11)	-0 (0.4)	0 (0.1)	0 (0.1)
	initial strain	30600*	3 (13)	-5 (13)	2 (11)	1 (0.5)	0 (0.2)	1 (0.2)
A46	Pearlite	0	40 (22)	-23 (17)	-17 (14)	-1 (0.9)	3 (1.4)	2 (0.7)
	-0.0075	100	10 (13)	-6 (13)	-4 (11)	1 (0.4)	0 (0.2)	0 (0.2)
	initial strain	24420*	0 (13)	-3 (13)	3 (11)	-1 (0.4)	0 (0.2)	1 (0.2)
A19	Spheroidite	0	3 (13)	-1 (13)	-2 (11)	-1 (0.4)	0 (0.1)	0 (0.2)
	No initial	100	13 (13)	-7 (13)	-5 (11)	0 (0.4)	0 (0.1)	0 (0.1)
	strain	10390*	3 (13)	-2 (13)	-1 (11)	-1 (0.3)	0 (0.1)	0 (0.1)
A20	Spheroidite	0	-45 (20)	28 (16)	17 (13)	1 (0.7)	1 (0.3)	0 (0.3)
	+0.0075	100	12 (13)	-7 (13)	-5 (11)	0 (0.4)	0 (0.1)	0 (0.1)
	initial strain	12870*	10 (13)	-7 (13)	-3 (11)	-2 (0.3)	0 (0.1)	0 (0.1)
A26	Spheroidite	0	47 (20)	-29 (16)	-18 (13)	1 (0.5)	0 (0.2)	0 (0.2)
	-0.0075	100	15 (13)	-9 (13)	-6 (11)	0 (0.3)	0 (0.1)	0 (0.1)
	initial strain	15500*	7 (13)	-3 (13)	-4 (11)	-1 (0.3)	0 (0.1)	1 (0.1)
A42	Temp. Mart.	0	-1 (13)	0 (13)	1 (12)	0 (0.5)	1 (0.5)	-1 (0.4)
	No initial	100	1 (14)	-1 (14)	0 (13)	0 (0.6)	0 (0.3)	0 (0.3)
	strain	99910	1 (14)	0 (14)	0 (13)	0 (0.6)	0 (0.3)	0 (0.4)
A37	Temp. Mart.	0	-10 (19)	7 (17)	3 (16)	-2 (1.6)	0 (0.5)	-1 (0.8)
	+0.005	100	-6 (15)	2 (15)	4 (14)	-2 (0.8)	1 (0.4)	0 (0.4)
	initial strain	100000	-5 (16)	2 (15)	3 (14)	1 (1.1)	0 (0.4)	0 (0.4)
A41	Temp. Mart.	0	7 (16)	-3 (14)	-4 (13)	0 (0.6)	0 (0.3)	0 (0.3)
	-0.005	100	3 (14)	0 (14)	-2 (13)	-1 (0.6)	0 (0.3)	0 (0.3)
	initial strain	100000	2 (14)	-1 (14)	-2 (13)	0 (0.6)	0 (0.3)	0 (0.3)

Table 4. Stresses after fatigue at 345 MPa.

(c) Deviatoric Microstresses Cementite (MPa)

Specimen		Cycles	$\mu_T c_{11}$	$\mu_T c_{22}$	$\mu_T c_{33}$	$\mu_T c_{12}$	$\mu_T c_{13}$	$\mu_T c_{23}$
A47	Pearlite	0	-7 (16)	-7 (16)	14 (13)	0 (2)	1 (1)	1 (1)
	No initial	190	-60 (16)	38 (16)	21 (14)	5 (2)	-3 (1)	-4 (1)
	strain	27850*	-72 (19)	45 (19)	28 (16)	-8 (3)	-2 (1)	-8 (1)
A45	Pearlite	0	366 (62)	-150 (64)	-216 (51)	-85 (15)	-31 (5)	-29 (5)
	+0.0075	100	-48 (18)	31 (18)	17 (15)	3 (2)	-3 (1)	1 (1)
	initial strain	30600*	-21 (20)	34 (20)	-13 (16)	-9 (3)	3 (1)	-4 (1)
A46	Pearlite	0	-268 (40)	152 (35)	116 (29)	5 (6)	-22 (3)	-11 (2)
	-0.0075	100	-69 (20)	42 (19)	27 (16)	-6 (3)	0 (1)	-2 (1)
	initial strain	24420*	3 (20)	18 (20)	-20 (16)	9 (3)	-1 (1)	-5 (1)
A19	Spheroidite	0	-16 (15)	5 (15)	11 (12)	4 (2)	0 (1)	2 (1)
	No initial	100	-73 (15)	43 (15)	31 (13)	0 (2)	2 (1)	1 (1)
	strain	10390*	-17 (14)	10 (14)	6 (12)	6 (2)	-2 (1)	2 (1)
A20	Spheroidite	0	264 (24)	-167 (21)	-97 (16)	-6 (4)	-4 (1)	-3 (2)
	+0.0075	100	-71 (16)	43 (16)	28 (13)	0 (2)	-1 (1)	3 (1)
	initial strain	12870*	-56 (15)	39 (14)	17 (12)	14 (2)	1 (1)	1 (1)
A26	Spheroidite	0	-274 (25)	168 (21)	105 (16)	-3 (3)	-1 (1)	-2 (1)
	-0.0075	100	-90 (15)	55 (15)	35 (13)	0 (2)	-3 (1)	0 (1)
	initial strain	15500*	-41 (14)	19 (14)	22 (12)	8 (2)	1 (1)	-5 (1)
A42	Temp. Mart.	0	17 (31)	5 (30)	-22 (34)	-2 (7)	-12 (3)	9 (3)
	No initial	100	-19 (44)	11 (45)	8 (51)	-3 (10)	-2 (4)	-1 (4)
	strain	99910	-10 (43)	8 (46)	2 (52)	3 (10)	-3 (4)	7 (4)
A37	Temp. Mart.	0	157 (71)	-113 (71)	-44 (83)	28 (18)	-8 (6)	14 (7)
	+0.005	100	94 (59)	-33 (65)	-61 (74)	36 (14)	-14 (6)	6 (5)
	initial strain	100000	75 (59)	-31 (59)	-45 (70)	-18 (14)	-3 (5)	-2 (5)
A41	Temp. Mart.	0	-117 (39)	56 (38)	61 (44)	-7 (9)	2 (3)	-1 (3)
	-0.005	100	-49 (43)	8 (42)	41 (49)	14 (10)	0 (4)	-3 (4)
	initial strain	100000	-36 (42)	10 (43)	26 (49)	-2 (10)	4 (4)	-4 (4)

Table 4. Stresses after fatigue at 345 MPa.

(d) Hydrostatic Stresses (MPa)

Specimen		Cycles	σ_{kk}	σ_{kk}^{α}	σ_{kk}^{γ}
A47	Pearlite	0	38 (91)	-74 (39)	502 (165)
	No initial	190	-99 (87)	-11 (24)	72 (162)
	strain	27850*	-142 (87)	-4 (24)	30 (162)
A45	Pearlite	0	4 (92)	-81 (41)	545 (166)
	+0.0075	100	-96 (87)	-8 (24)	56 (162)
	initial strain	30600*	-90 (87)	-2 (24)	12 (162)
A46	Pearlite	0	-89 (87)	-9 (24)	61 (162)
	-0.0075	100	-68 (87)	-9 (24)	59 (162)
	initial strain	24420*	-103 (87)	-1 (24)	12 (162)
A19	Spheroidite	0	40 (48)	-16 (13)	95 (70)
	No initial	100	-29 (47)	-6 (12)	36 (70)
	strain	10390*	-27 (47)	14 (12)	-80 (70)
A20	Spheroidite	0	8 (47)	-11 (12)	63 (70)
	+0.0075	100	-39 (47)	-3 (12)	18 (70)
	initial strain	12870*	18 (47)	11 (12)	-66 (70)
A26	Spheroidite	0	-50 (47)	1 (12)	-5 (70)
	-0.0075	100	-53 (47)	-3 (12)	17 (70)
	initial strain	15500*	-39 (47)	18 (12)	-103 (70)
A42	Temp. Mart.	0	9 (47)	0 (6)	-4 (106)
	No initial	100	0 (47)	2 (6)	-36 (106)
	strain	99910	-2 (48)	4 (7)	-72 (106)
A37	Temp. Mart.	0	-85 (48)	-17 (13)	277 (107)
	+0.005	100	-47 (47)	3 (6)	-44 (106)
	initial strain	100000	-37 (47)	0 (6)	-10 (106)
A41	Temp. Mart.	0	73 (48)	7 (8)	-114 (106)
	-0.005	100	47 (47)	-1 (6)	23 (106)
	initial strain	100000	31 (47)	4 (7)	-69 (106)

Numbers in parentheses are the sum in quadrature of the instrumental, statistical, and volume fraction errors.

*Indicates that the specimen broke.

Figure Captions

Figure 1. Coordinate systems used in diffraction measurements of stress. The S_i coordinate system is the specimen coordinate system and is the one to which measured stress tensors are referred. The L_i coordinate system is the laboratory coordinate system in which the diffraction measurements are made. Lattice spacings are measured along the L_3 axis by placing the diffraction vector along it.

Figure 2. Specimen geometries for (a) fatigue at 276 MPa and (b) fatigue at 345 MPa. Dimensions in mm.

Figure 3. Macrostresses and microstresses along the loading direction with fatigue at 276 MPa in (a) pearlite, (b) spheroidite, and (c) tempered martensite. Error bar shows a typical error in the microstresses in the cementite phase. Errors in the macrostresses and microstresses in the ferrite phase are within the symbol size.

Figure 4. Macrostresses and microstresses along the loading direction in a shot peened spheroidite fatigued at 276 MPa. Error bar shows a typical error in the microstresses in the cementite phase. Errors in the macrostresses and microstresses in the ferrrite phase are within the symbol size.

Figure 5. Macrostresses and microstresses along the loading direction in pearlite with fatigue at 345 MPa. for (a) no initial strain, (b) +0.0075 initial strain, and (c) -0.0075 initial strain. Error bar shows a typical error in the microstresses in the cementite phase. Errors in the macrostresses and microstresses in the ferrrite phase are within the symbol size.

Figure 6. Macrostresses and microstresses along the loading direction in spheroidite with fatigue at 345 MPa. for (a) no initial strain, (b) +0.0075 initial strain, and (c) -0.0075 initial strain. Error bar shows a typical error in the microstresses in the cementite phase. Errors in the macrostresses and microstresses in the ferrrite phase are within the symbol size.

Figure 7. Macrostresses and microstresses along the loading direction in tempered martensite with fatigue at 345 MPa. for (a) no initial strain, (b) +0.005 initial strain, and (c) -0.005 initial strain. Error bar shows a typical error in the microstresses in the cementite phase. Errors in the macrostresses and microstresses in the ferrrite phase are within the symbol size.

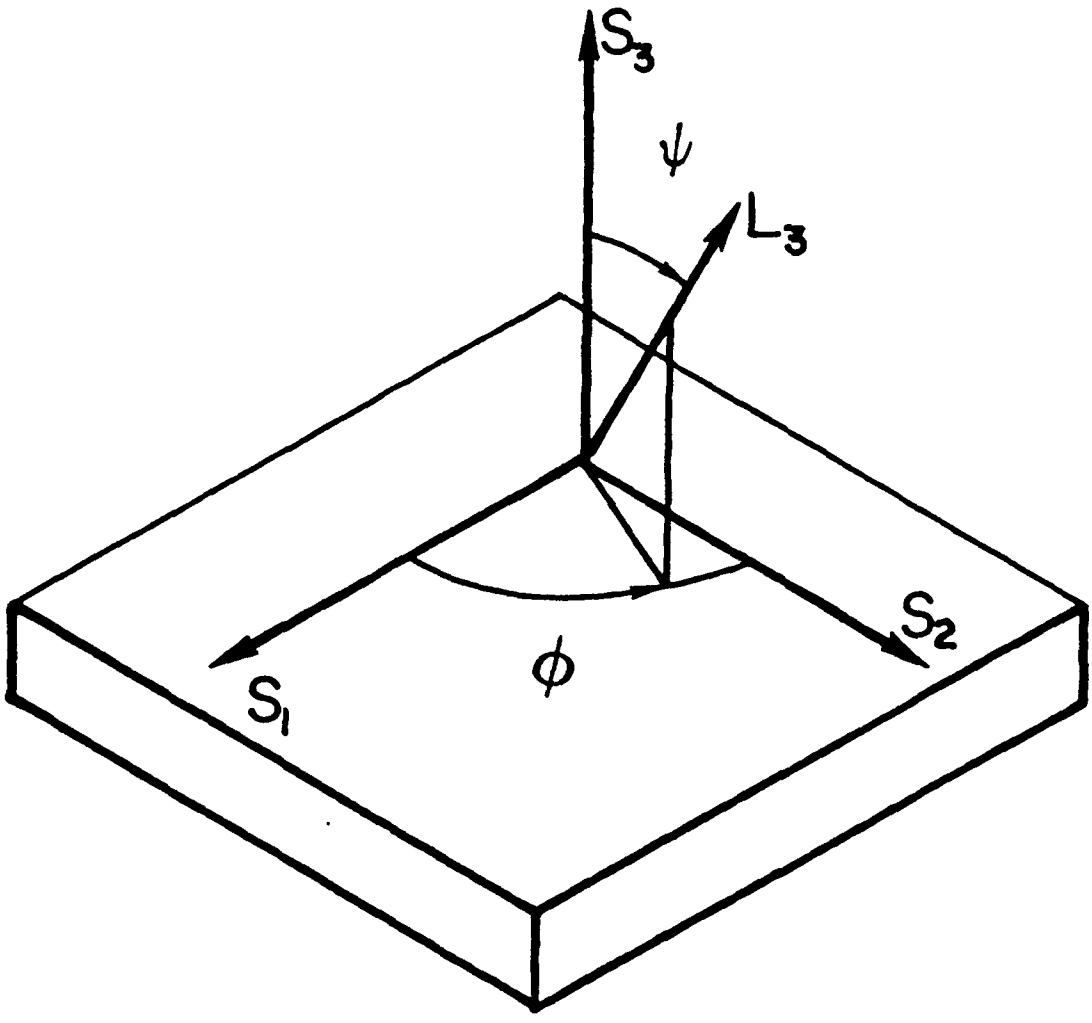

Figure 1. Coordinate systems used in diffraction measurements of stress. The S_i coordinate system is the specimen coordinate system and is the one to which measured stress tensors are referred. The L_i coordinate system is the laboratory coordinate system in which the diffraction measurements are made. Lattice spacings are measured along the L_3 axis by placing the diffraction vector along it.

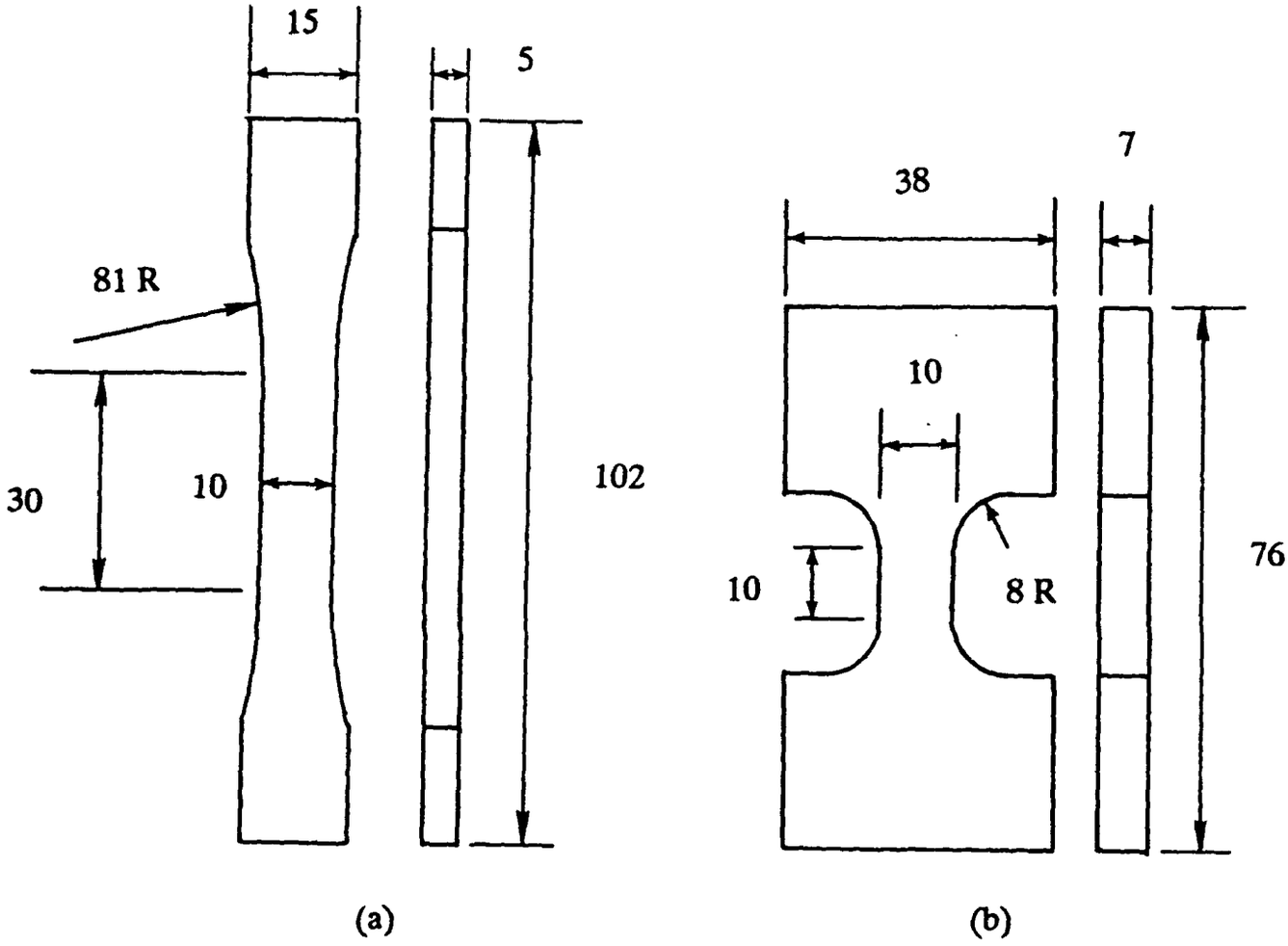

Figure 2. Specimen geometries for (a) fatigue at 276 MPa and (b) fatigue at 345 MPa. Dimensions in mm.

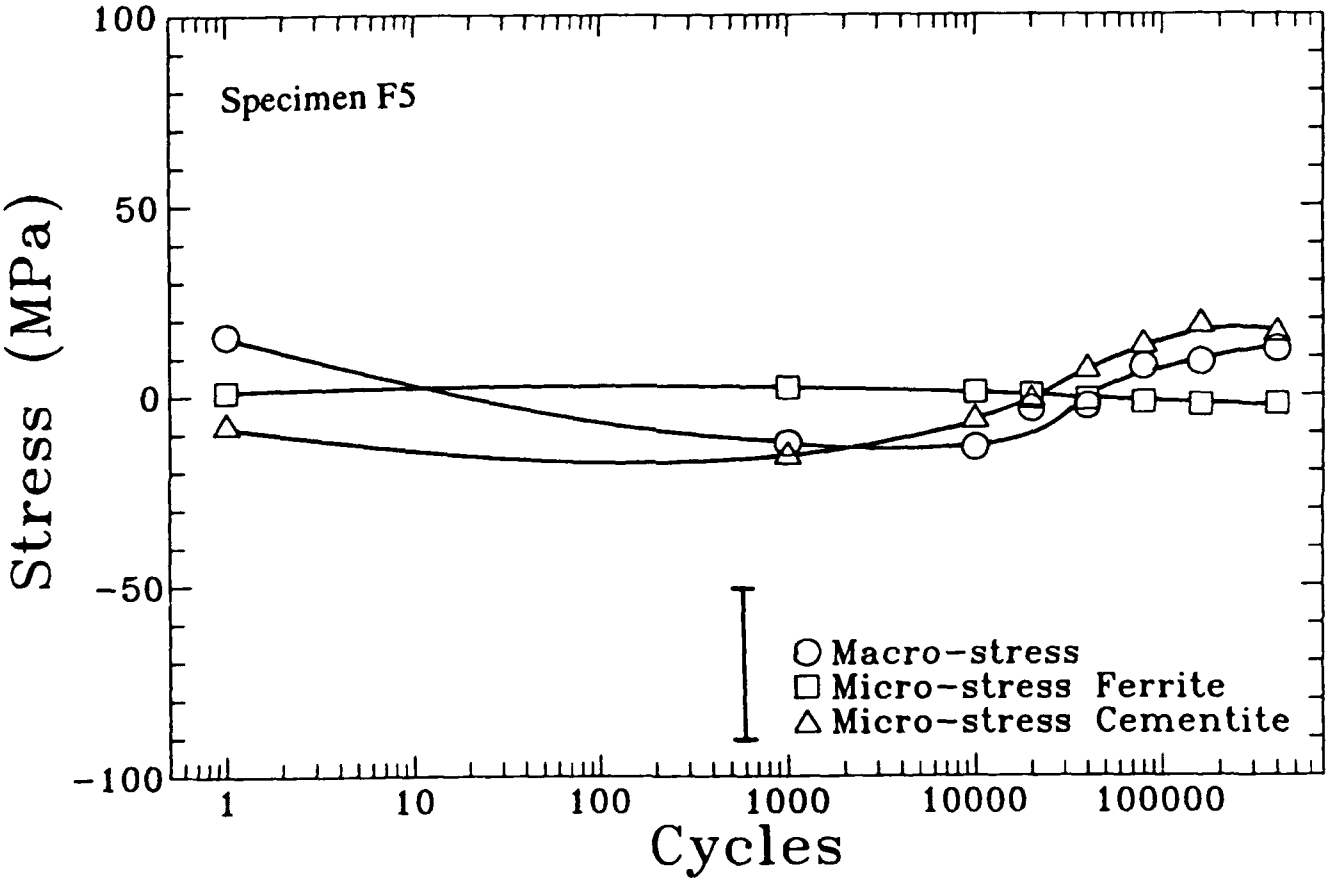

Figure 3 (a)

Figure 3. Macrostresses and microstresses along the loading direction with fatigue at 276 MPa in (a) pearlite, (b) spheroidite, and (c) tempered martensite. Error bar shows a typical error in the microstresses in the cementite phase. Errors in the macrostresses and microstresses in the ferrite phase are within the symbol size.

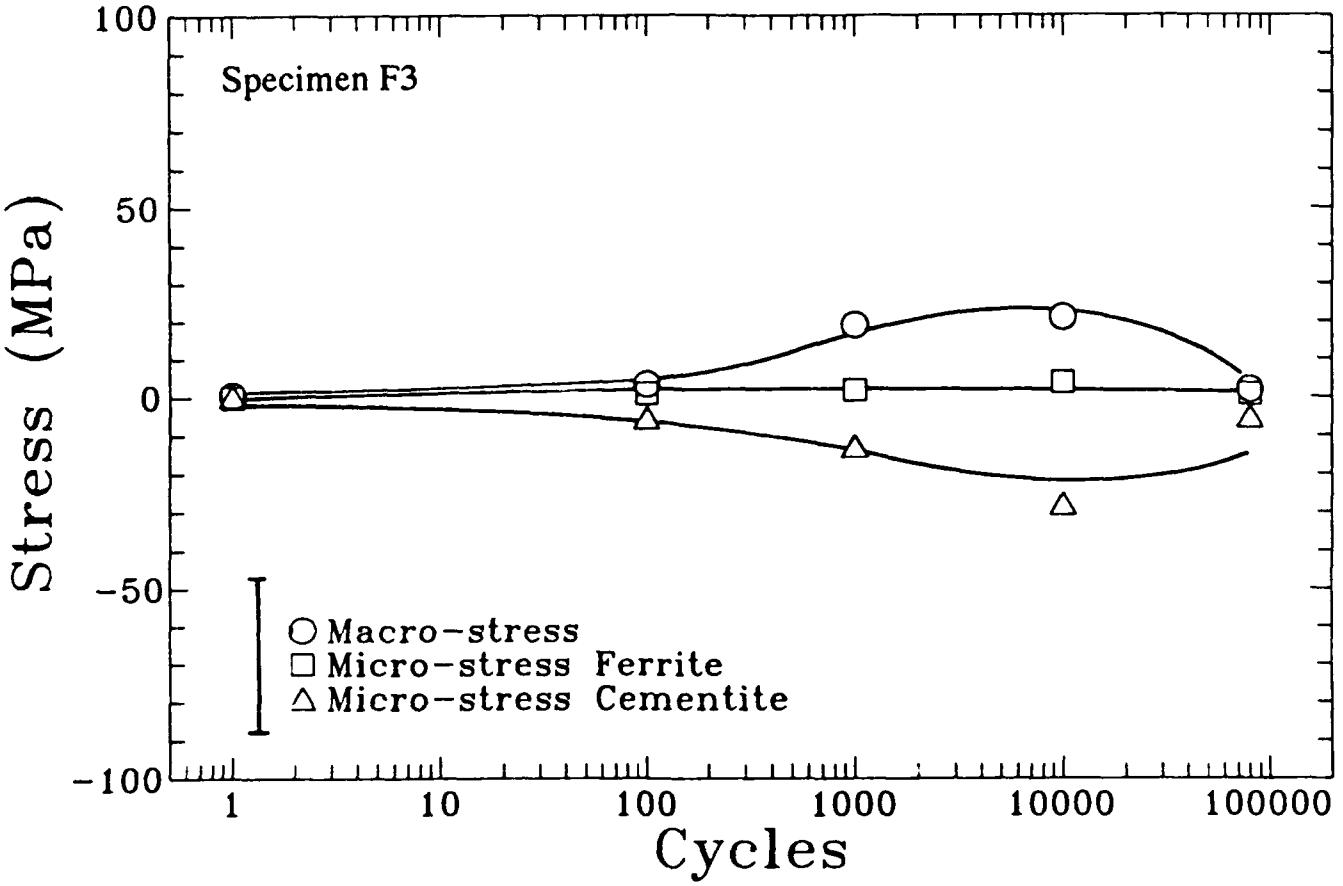
Specimen F3
Stress (MPa)
100
50
0
-50
-100
1
10
100
1000
10000
100000
Cycles
Macro-stress
Micro-stress Ferrite
Micro-stress Cementite

Figure 3 (b)

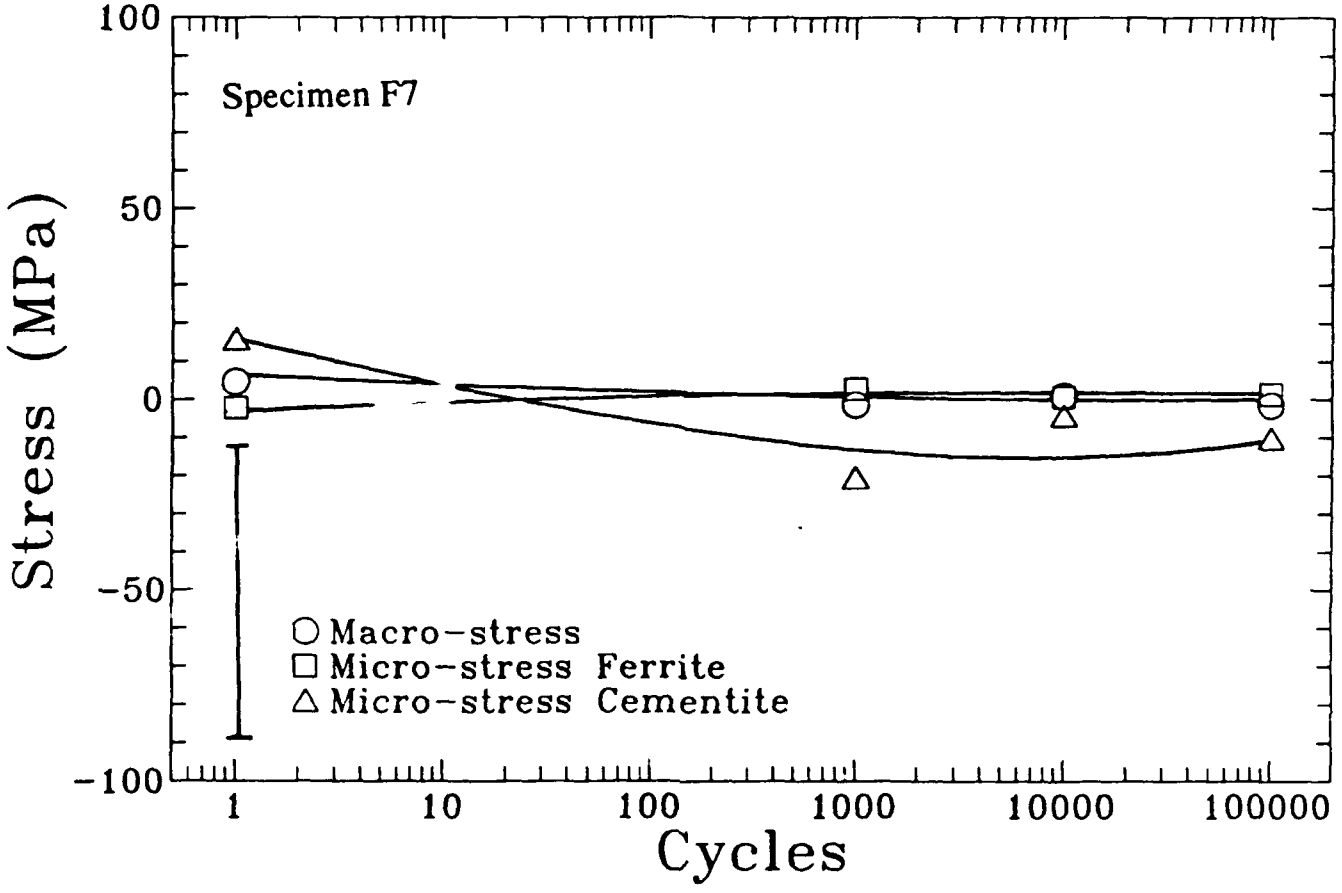
Specimen F7
Stress (MPa)
100
50
0
-50
-100
1
10
100
1000
10000
100000
Cycles
Macro-stress
Micro-stress Ferrite
Micro-stress Cementite

Figure 3 (c)

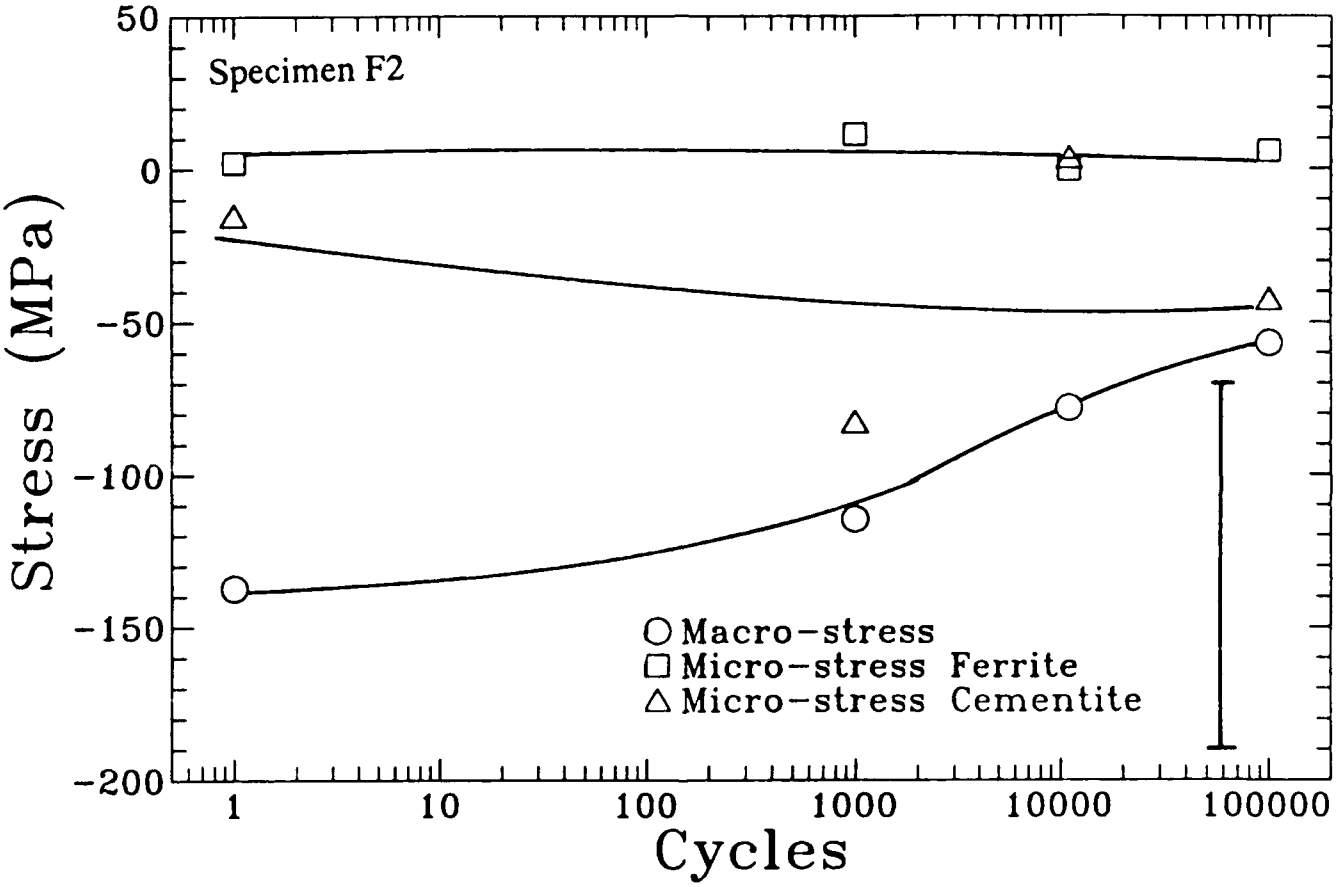

Figure 4. Macrostresses and microstresses along the loading direction in a shot peened spheroidite fatigued at 276 MPa. Error bar shows a typical error in the microstresses in the cementite phase. Errors in the macrostresses and microstresses in the ferrrite phase are within the symbol size.

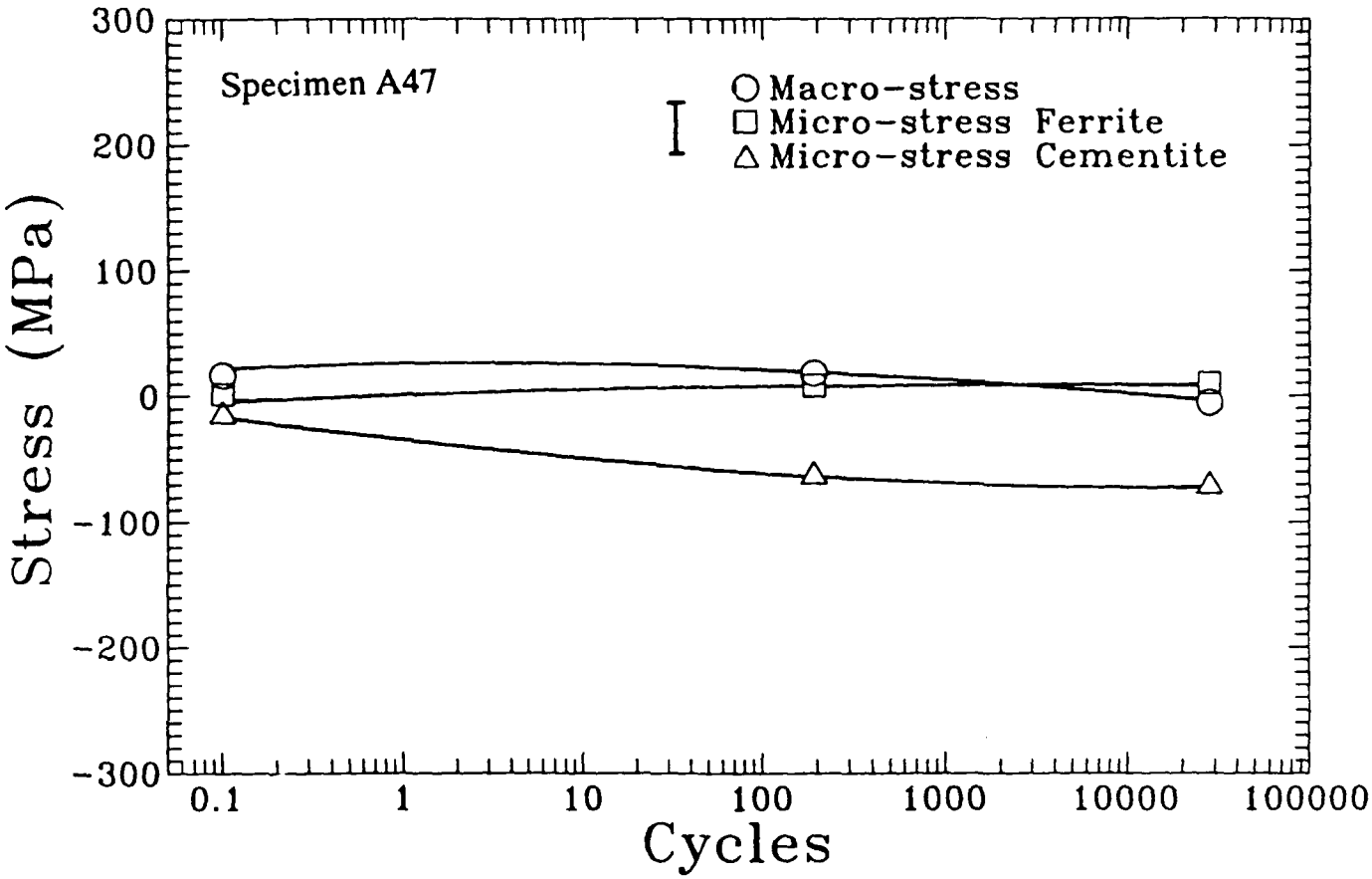

Figure 5 (a)

Figure 5. Macrostresses and microstresses along the loading direction in pearlite with fatigue at 345 MPa. for (a) no initial strain, (b) +0.0075 initial strain, and (c) -0.0075 initial strain. Error bar shows a typical error in the microstresses in the cementite phase. Errors in the macrostresses and microstresses in the ferrrite phase are within the symbol size.

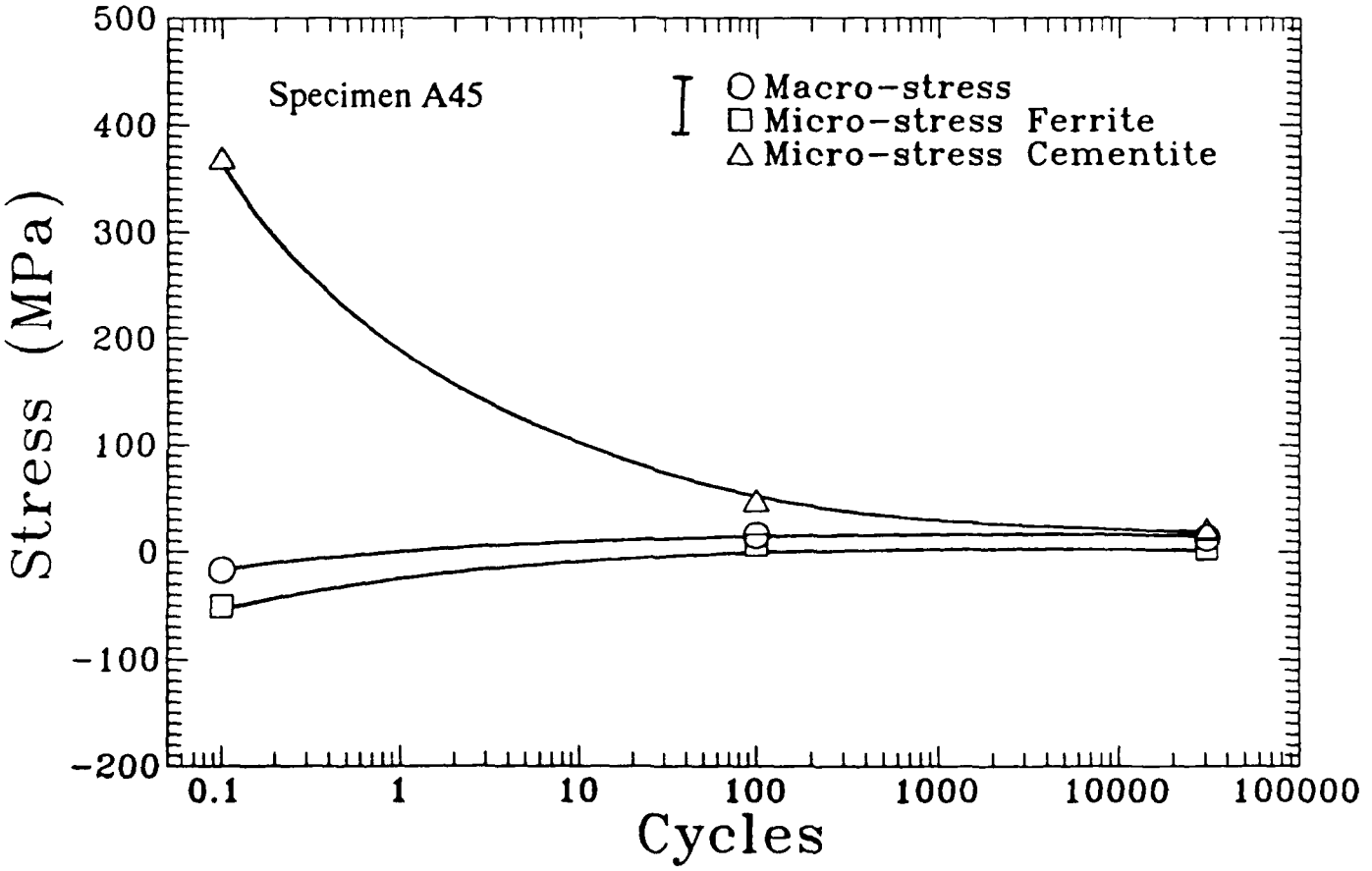
Specimen A45
Macro-stress
Micro-stress Ferrite
Micro-stress Cementite
Stress (MPa)
500
400
300
200
100
0
-100
-200
0.1
1
10
100
1000
10000
100000
Cycles

Figure 5 (b)

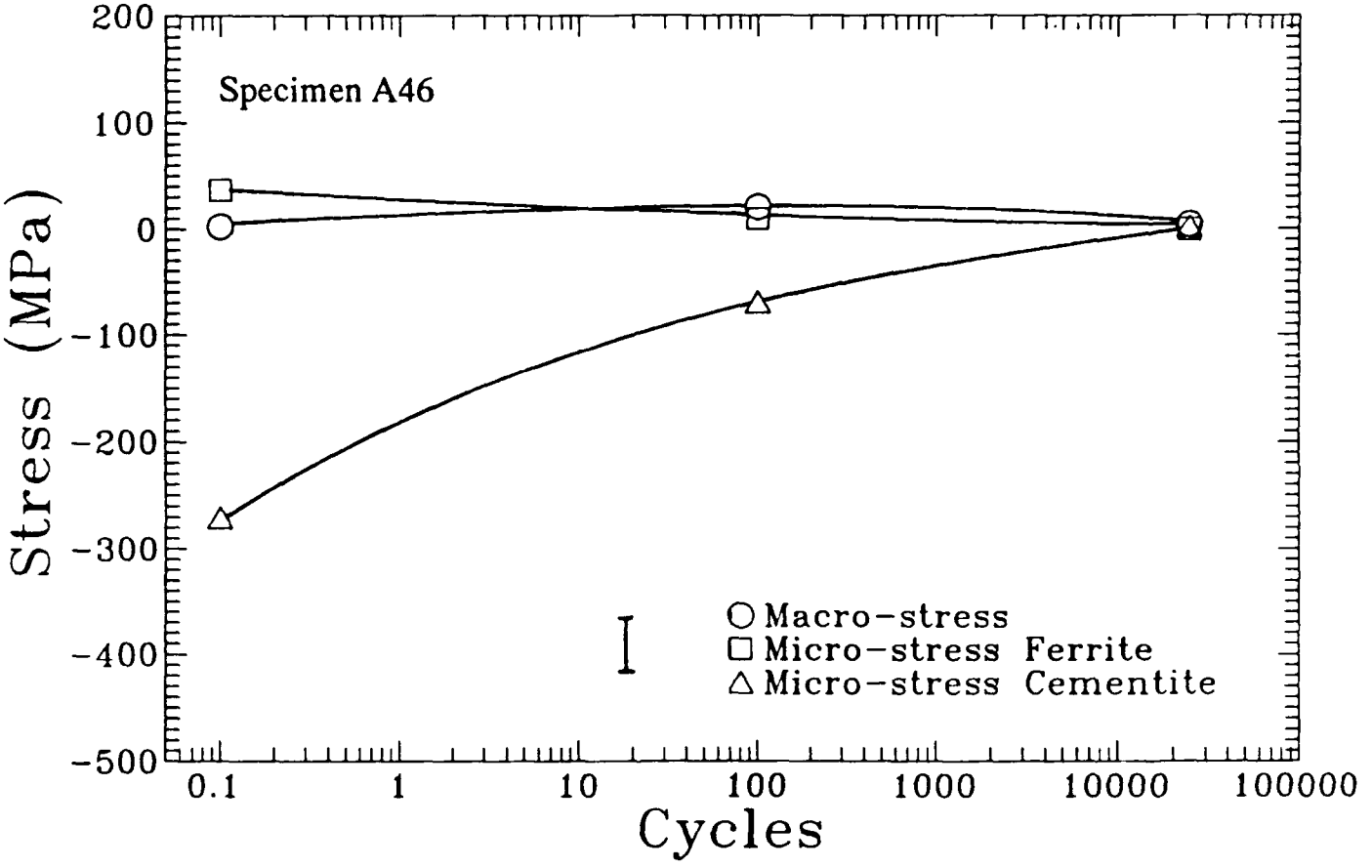
Specimen A46
Stress (MPa)
200
100
0
-100
-200
-300
-400
-500
0.1
1
10
100
1000
10000
100000
Cycles
Macro-stress
Micro-stress Ferrite
Micro-stress Cementite

Figure 5 (c)

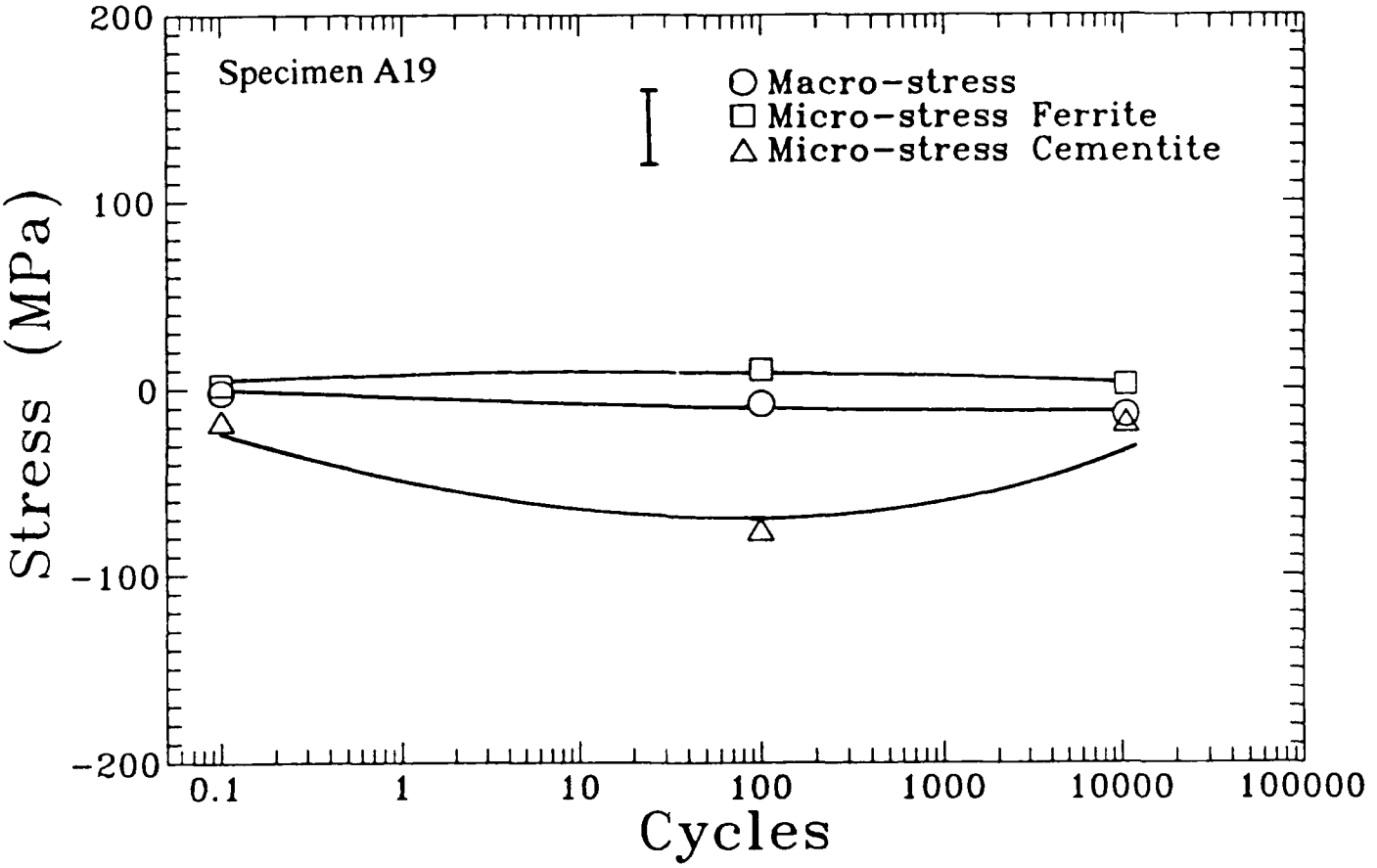

Figure 6 (a)

Figure 6. Macrostresses and microstresses along the loading direction in spheroidite with fatigue at 345 MPa. for (a) no initial strain, (b) +0.0075 initial strain, and (c) -0.0075 initial strain. Error bar shows a typical error in the microstresses in the cementite phase. Errors in the macrostresses and microstresses in the ferrrite phase are within the symbol size.

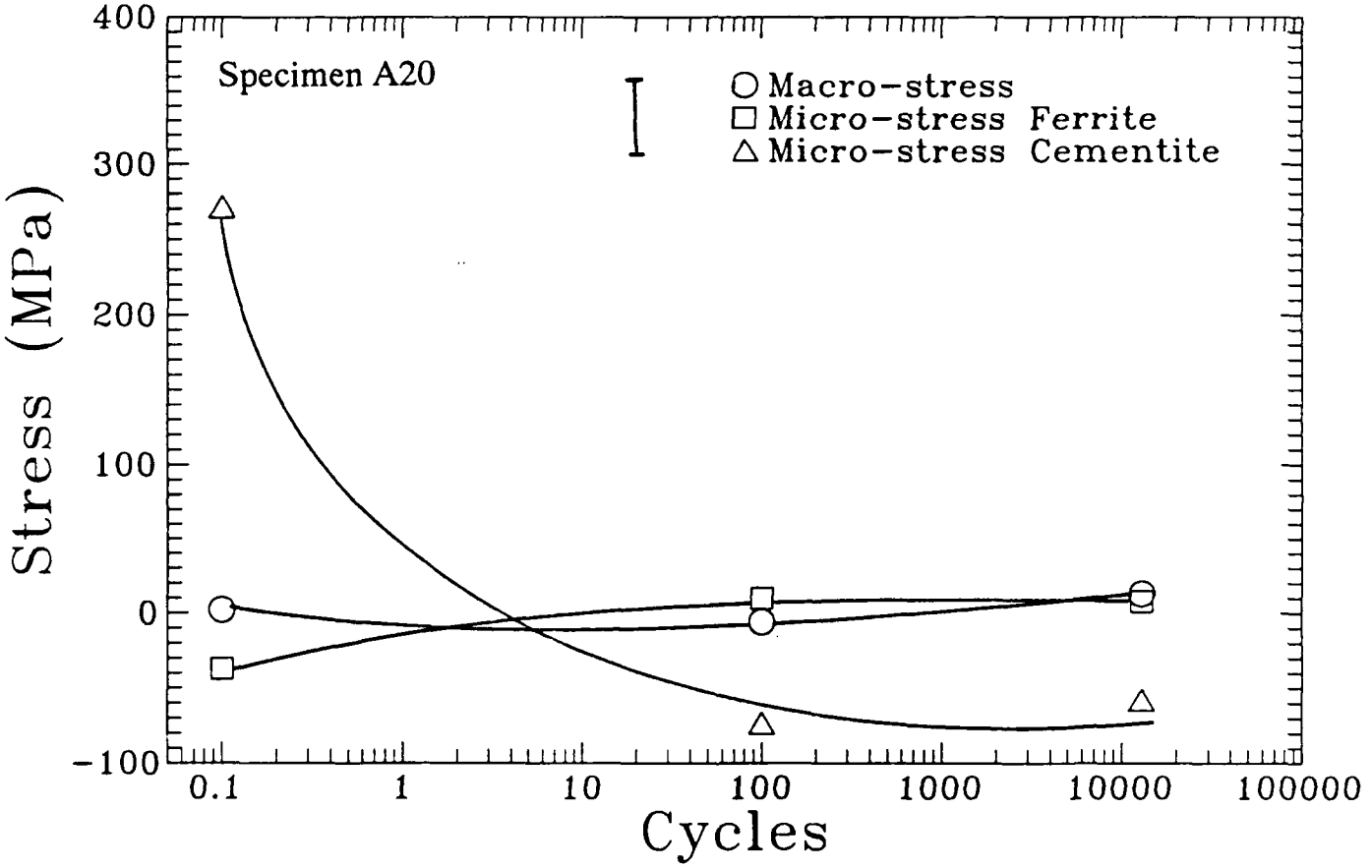
Specimen A20
Macro-stress
Micro-stress Ferrite
Micro-stress Cementite
Stress (MPa)
400
300
200
100
0
-100
0.1
1
10
100
1000
10000
100000
Cycles

Figure 6 (b)

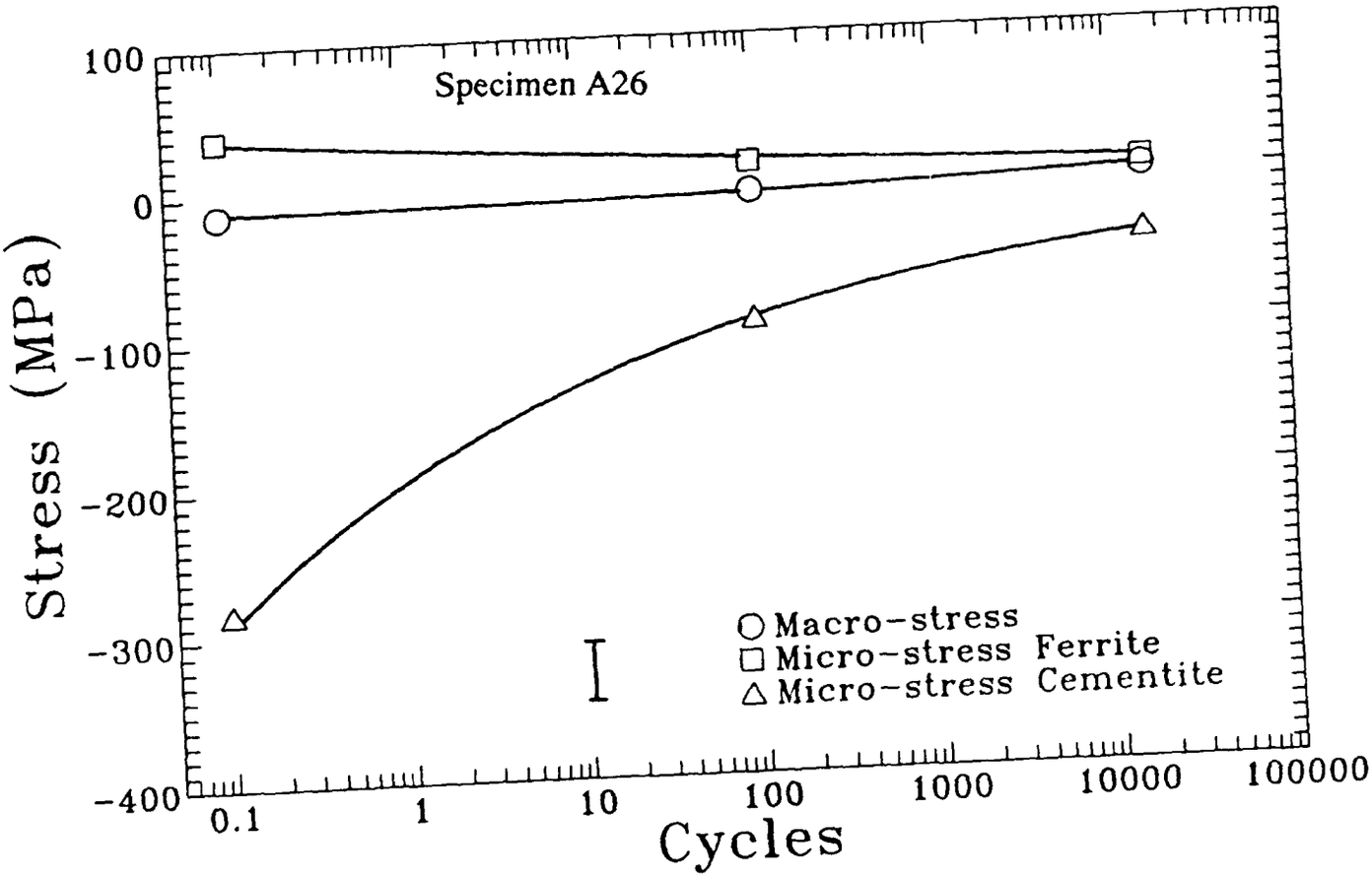
Specimen A26
100
0
-100
-200
-300
-400
Stress (MPa)
0.1
1
10
100
1000
10000
100000
Cycles
Macro-stress
Micro-stress Ferrite
Micro-stress Cementite

Figure 6 (c)

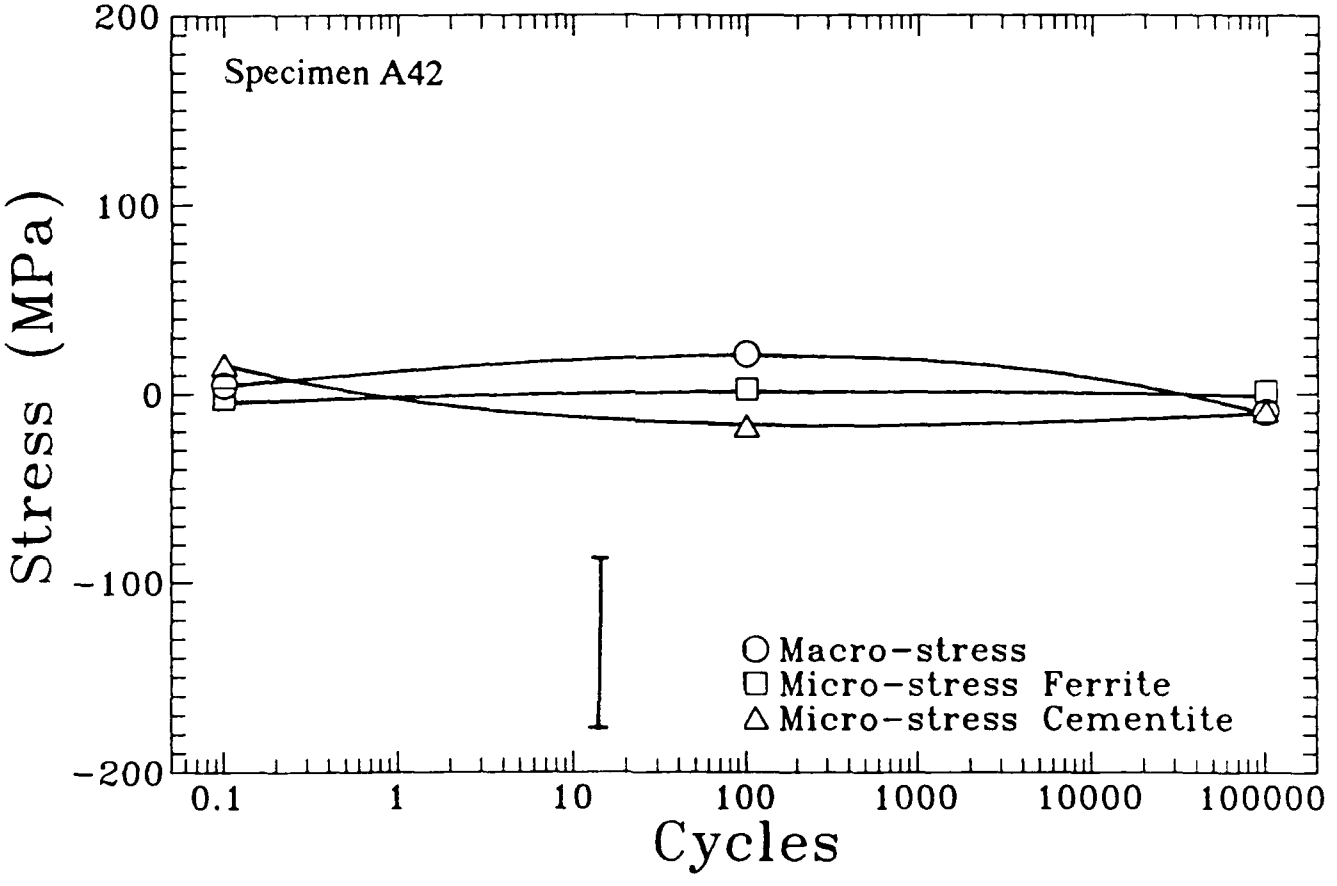

Figure 7 (a)

Figure 7. Macrostresses and microstresses along the loading direction in tempered martensite with fatigue at 345 MPa. for (a) no initial strain, (b) +0.005 initial strain, and (c) -0.005 initial strain. Error bar shows a typical error in the microstresses in the cementite phase. Errors in the macrostresses and microstresses in the ferrrite phase are within the symbol size.

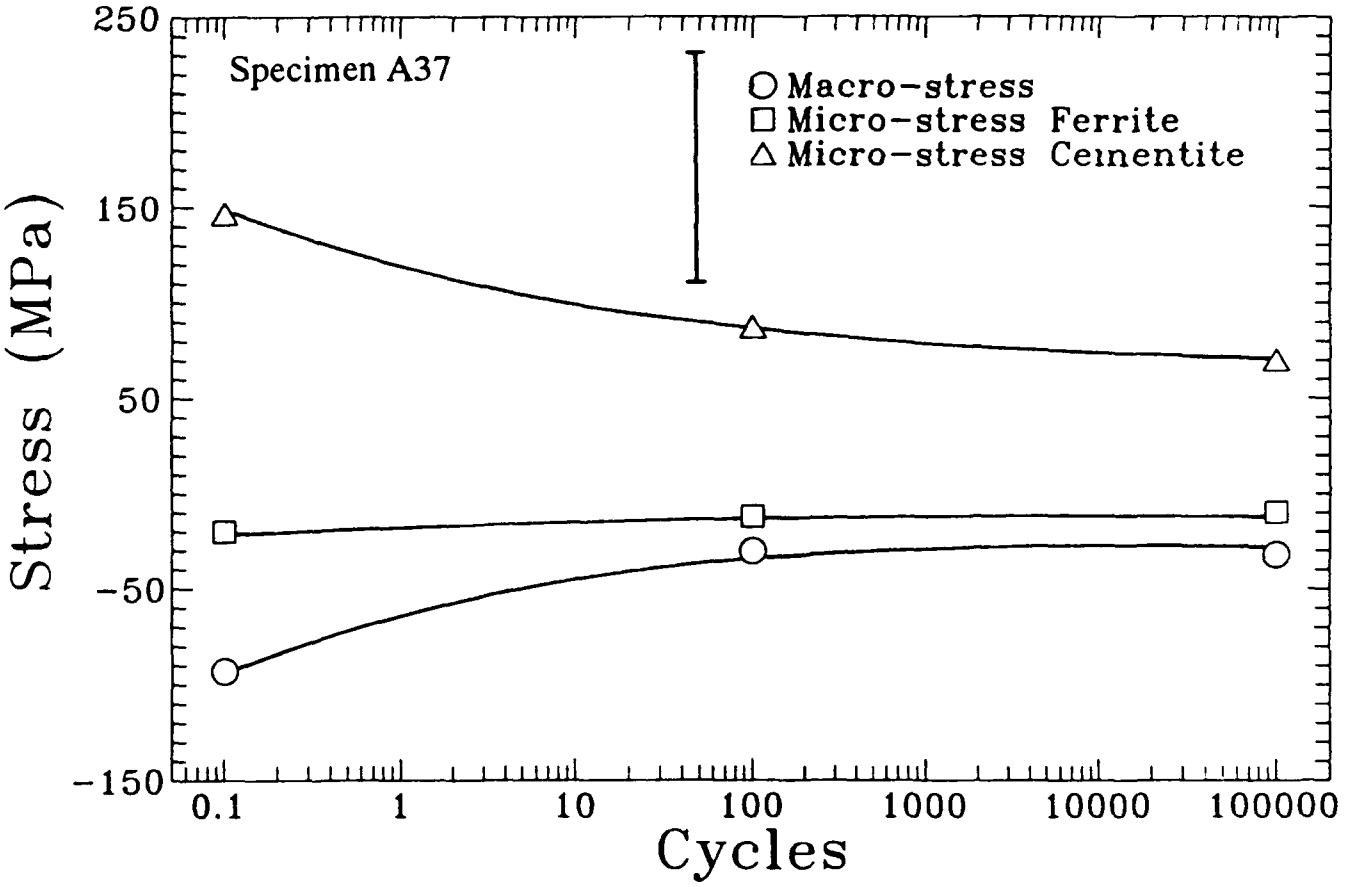
Specimen A37
Macro-stress
Micro-stress Ferrite
Micro-stress Cementite
Stress (MPa)
250
150
50
-50
-150
0.1
1
10
100
1000
10000
100000
Cycles

Figure 7 (b)

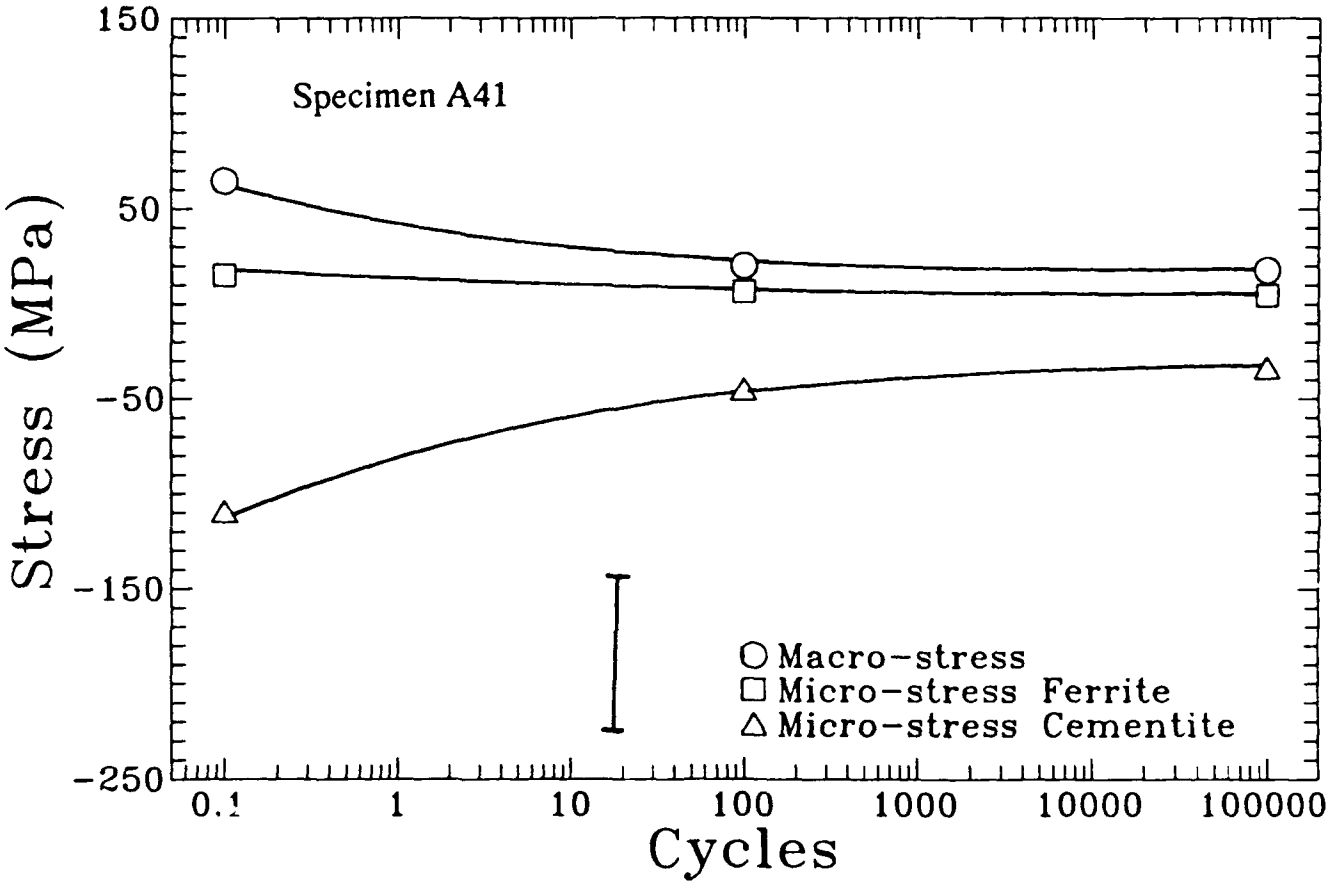
Specimen A41
150
50
-50
-150
-250
Stress (MPa)
0.1
1
10
100
1000
10000
100000
Cycles
Macro-stress
Micro-stress Ferrite
Micro-stress Cementite

Figure 7 (c)

Security Classification

DOCUMENT CONTROL DATA - R & D

(Security classification of title, body of abstract and indexing annotation must be entered when the overall report is classified)

1. ORIGINATING ACTIVITY (Corporate author)

J.B. Cohen
McCormick School of Engineering & Applied Science
Northwestern University, Evanston, IL 60208

2a. REPORT SECURITY CLASSIFICATION

2b. GROUP

3. REPORT TITLE

CHANGES IN THE MACROSTRESSES AND MICROSTRESSES IN STEEL WITH FATIGUE

4. DESCRIPTIVE NOTES (Type of report and inclusive dates)

TECHNICAL REPORT #32

5. AUTHOR(S) (First name, middle initial, last name)

J.B. Cohen and R.A. Winholtz

6. REPORT DATE

July 1991

7a. TOTAL NO. OF PAGES

48 pages

7b. NO. OF REFS

8a. CONTRACT OR GRANT NO.

b. PROJECT NO.

c.

d.

9a. ORIGINATOR'S REPORT NUMBER(S)

32

9b. OTHER REPORT NO(S) (Any other numbers that may be assigned this report)

10. DISTRIBUTION STATEMENT

Distribution of document is unlimited

11. SUPPLEMENTARY NOTES

12. SPONSORING MILITARY ACTIVITY

Metallurgy Branch
Office of Naval Research

13. ABSTRACT

The residual stresses in both the ferrite and cementite phases of fatigued 1080 steel specimens with pearlite, spheroidite, and tempered martensite microstructures were measured with x-ray diffraction giving both the macrostresses and the microstresses. Specimens with no initial stresses showed little changes with fatigue. Specimens with initial macrostresses and with initial microstresses showed fading of the stresses, the fading being the slowest for the strongest microstructure. Hydrostatic microstresses are present after heat treatment due to the differential thermal properties of the cementite and ferrite.

KEY WORDS	LINK A		LINK B		LINK C	
	ROLE	WT	ROLE	WT	ROLE	WT

DD FORM 1 NOV 68 1473 (BACK)
(PAGE 2)